ELSEVIER

Review

A review of modern transition-metal nanoclusters: their synthesis, characterization, and applications in catalysis

John D. Aiken III, Richard G. Finke *

Department of Chemistry, Colorado State University, Ft. Collins, CO 80523, USA

Abstract

A literature review of modern transition-metal nanoclusters, with an emphasis on those nanoclusters which are catalytically active, is presented in two parts. Part One presents background information on transition-metal nanoclusters, including an overview of common synthetic routes, a description of how nanoclusters are stabilized, and a brief summary of the multiple characterization techniques used (and the type of information that they can provide). In Part Two, five specific nanocluster case studies are presented, case studies which compare and contrast the syntheses, characterization approaches, and catalytic applications of transition-metal nanoclusters. © 1999 Elsevier Science B.V. All rights reserved.

1. Introduction

Nanoclusters—near monodispersed particles that are generally less than 10 nm (100 Å) in diameter [1]—have generated intense interest over the past decade. One reason for this is the belief that nanoclusters will have unique properties, derived in part from the fact that these particles and their properties lie somewhere between those of bulk and single-particle species [2,3]. Such 'strange morsels of matter' [4] have many fascinating potential uses, including quantum dots [5] or quantum computers [6] and devices [7,8], chemical sensors [9], light-emitting diodes [10], 'ferrofluids' for cell separations [11], industrial lithography [12], and photochemical pattern applications such as flat-panel displays [13]. Nanoclusters also have significant potential as new types of higher activity and selectivity catalysts [14–35]. For example, important work from Schmid's laboratories gives a glimpse of the unusual catalytic selectivities that nanoclusters promise to provide [14].

Two reasons chemists believe that nanoclusters hold the potential to be more active and selective catalysts than those of today are that a large percentage of a nanocluster's metal atoms lie on the surface, and that surface atoms do not necessarily order themselves in the same way that those in the

---

* Corresponding author

bulk do [4]. Furthermore, the electrons in a nanocluster are confined to spaces that can be as small as a few atom-widths across, giving rise to quantum size effects [4]. Perhaps most importantly, nanoclusters offer the possibility of controlling both the nanocluster size and the surface ligands in a quantitative, modifiable and better understood way than previously possible for, say, supported heterogeneous catalysts.

Nanoclusters have been found to catalyze a range of reactions, spanning hydrogenations [15]; enantioselective hydrogenations [16]; hydrosilylations [17]; hydropyrolysis and hydrogenolysis [18]; oxidation of CO and CO/H_2 [19]; oxidative acetoxylation [20]; McMurry [21], Suzuki [22], and Heck-Type [23] couplings; and, most recently, [3 + 2] cycloaddition reactions [24]. The majority of these reactions have been performed by nanoclusters deposited on a heterogeneous support; there are only two well-characterized nanocluster systems (Moiseev's $Pd_{\sim 570}$ nanoclusters [20], and poly-oxoanion-stabilized Ir(0) and Rh(0) nanoclusters [1]) in which the nanoclusters can be isolated and then redissolved while retaining their catalytic activity *and* which exhibit significant lifetimes *in solution* [1]. Only one of those systems has a proven catalytic lifetime in solution of $\geq 190,000$ turnovers, and that system will be discussed towards the end of the review, including the source of its nanocluster stabilizer.

This review, then, is organized into two parts: Part One (Section 2) presents fundamental background information on nanoclusters, including how they can be synthesized, stabilized against aggregation, and characterized; a bit of discussion of non-transition metal nanoclusters is provided in places where it helps give a broader perspective of the state of nanocluster science. Part Two (Section 3) presents five Case Studies, providing specific details on the synthesis, characterization, and catalytic studies of five literature prototype nanocluster systems. An outlook for the future is provided at the end of the review (Section 5).

2. Part One. Fundamental background information

2.1. Methods used to synthesize nanoparticles

Nanoparticles have been synthesized by a variety of methods [1]. Common synthetic techniques for *semiconductor* nanoparticles employ the use of constrained environments, such as inverse micelles [25–30]; [1] capping agents, which arrest the growth of particles when they reach a certain size [31]; zeolites, ionomers, porous glass [32] and gels [31]; solid polymer environments [33,34]; or dendrimers [35]. For *transition metal* nanoclusters, however, Professor John Bradley points out that there are four general synthetic methods; the key requirement of each is that it result in the 'facile deposition of metallic precipitates' [48]. These four methods are: (i) transition metal salt reduction, (ii) thermal decomposition and photochemical methods, (iii) ligand reduction and displacement from organometallics, and (iv) metal vapor synthesis. Not included on Bradley's list, however, is a fifth, recent category of (v) electrochemical synthesis developed by Professor Manfred Reetz, an important method discussed in more detail in Part Two. Methods (i), (iii) and (v) have been proven to be convenient for growing *isolable* transition metal nanoclusters that can be redissolved in non-aqueous solution, and, hence, are most relevant to this review.

---

[1] Examples of nanoparticles, and especially semiconductor nanoparticles, grown in inverse micelles include Refs. [36–46]. For a recent review, including a discussion of the effects of concentration and types of reducing agents, the effect of solvents and additives, and the kinetics and mechanism of formation of microparticles in reversed micelles, see Ref. [47].

Important goals in the nanocluster area include the development of reproducible syntheses of nanoclusters of a predetermined size, structure, shape, [2] and composition [2,3,52] (see also Ref. [53]). Unfortunately, efforts aimed at understanding the kinetics and mechanism of nanocluster formation—efforts which would ultimately allow *control* over these properties—have been lacking until very recently [52]. One reason for this dearth of mechanistic studies is that only recently have well-defined nanocluster systems become available which are even appropriate for in-depth kinetic and mechanistic studies. The polyoxoanion-stabilized nanocluster system discussed herein is one such system [52] and is the first modern nanocluster system for which in-depth kinetic and mechanistic studies of the nanocluster formation process have appeared.

2.2. Stabilization of nanoclusters against aggregation

Nanoclusters are only kinetically stable; they must be stabilized against aggregation into larger particles and, eventually, bulk material, their thermodynamic minimum. Stabilization can be accomplished in two precedented ways: electrostatic (charge, or 'inorganic') stabilization and steric ('organic') stabilization.

Electrostatic stabilization occurs by the adsorption of ions to the often electrophilic metal surface [54]. This adsorption creates an electrical double (really multi-) layer [55], which results in a Coulombic repulsion force between individual particles, Fig. 1.

Steric stabilization is achieved by surrounding the metal center by layers of material that are sterically bulky [54], such as polymers [56] or surfactants [57]. These large adsorbates provide a steric barrier which prevents close contact of the metal particle centers, Fig. 2.

Some nanocluster stabilizers combine both electrostatic *and* steric stabilization [1,15], as in the case of the polyoxoanion-stabilized nanoclusters presented in this review.

Interestingly, there have recently been reports of nanoclusters that are claimed to be stabilized by solvent molecules alone (such as ethers and thioethers), that is, in the absence of charge or steric stabilizers [23,57,59]. However, in some cases, proof of the absence of stabilizing anions or cations is lacking, or elemental analysis shows that Br^- or Cl^- still remain [57]. Two of these examples will be described in more detail in Part Two (Section 3) of this review.

2.3. Full shell ('magic number') metal clusters

Metal clusters which have a complete, regular outer geometry are designated full-shell, or 'magic number', clusters, Fig. 3. Full-shell clusters are constructed by successively packing layers—or shells—of metal atoms around a single metal atom. The total number of metal atoms, y, per nth shell is given by the equation $y = 10n^2 + 2$ $(n > 0)$ [60]. Thus, full-shell metal clusters contain M_{13} $(1 + 12 = 13)$, M_{55} $(13 + 42 = 55)$, M_{147} $(55 + 92 = 147)$, M_{309}, M_{561}, M_{923} (and so on) metal atoms.

Many nanocluster distributions center around one of these full-shell geometries. This is not too surprising; it is believed that full-shell clusters have added stability, as their densely-packed structures provide the maximum number of metal–metal bonds [52]. Recently Finke and Watzky have demonstrated an autocatalytic surface-growth mechanism of nanocluster formation for Ir nanoclusters,

---

[2] For a series of papers describing the formation of colloidal platinum nanoparticles of different shapes (cubic, tetrahedral, or truncated octahedral), see Refs. [49–51].
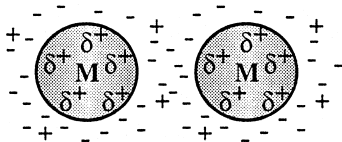
Fig. 1. Schematic image of two electrostatically-stabilized nanoparticles [1]. Ions adsorb onto the surface of the nanoparticles, creating an electrical double layer which provides Coulombic repulsion and thus stabilization against aggregation. The nature of the δ^+ 'charge mirror' is discussed elsewhere [1].

a mechanism that explains how full-shell clusters are formed and isolated in kinetically controlled syntheses (which all transition-metal nanocluster syntheses are, at least with respect to the thermodynamic sink of bulk metal [52]). Note, however, that because full-shell clusters have some degree of added stability they are expected to be *less active* catalysts [52].

2.4. Characterization techniques used in nanocluster chemistry

A key goal of nanocluster characterization is to establish particle size and overall composition. Surface composition is sometimes also probed, but this is a more formidable task. Fig. 4 provides a good overall picture of the techniques most often used to characterize nanoclusters [61].

Characterization techniques often used include transmission electron microscopy (TEM), UV–Visible spectroscopy (UV–Vis), nuclear magnetic resonance spectroscopy (NMR), infrared spectroscopy (IR), elemental analysis, and energy dispersive spectroscopy (EDS). To a lesser extent the following methods are used: analytical ultracentrifugation–sedimentation, extended X-ray absorption fine structure (EXAFS), scanning tunneling microscopy (STM), atomic force microscopy (AFM), high performance liquid chromatography (HPLC), light scattering, time-of-flight mass spectrometry, magnetic susceptibility, and electrophoresis or ion-exchange chromatography. Some of the more important and non-routine techniques applied in nanocluster characterization, and the type of structural or compositional information gained from them, are discussed next.

X-ray crystallography would be the ideal method of characterizing such molecules, but nanoclusters generally do not crystallize. It has been postulated that their often spherical shapes hinder
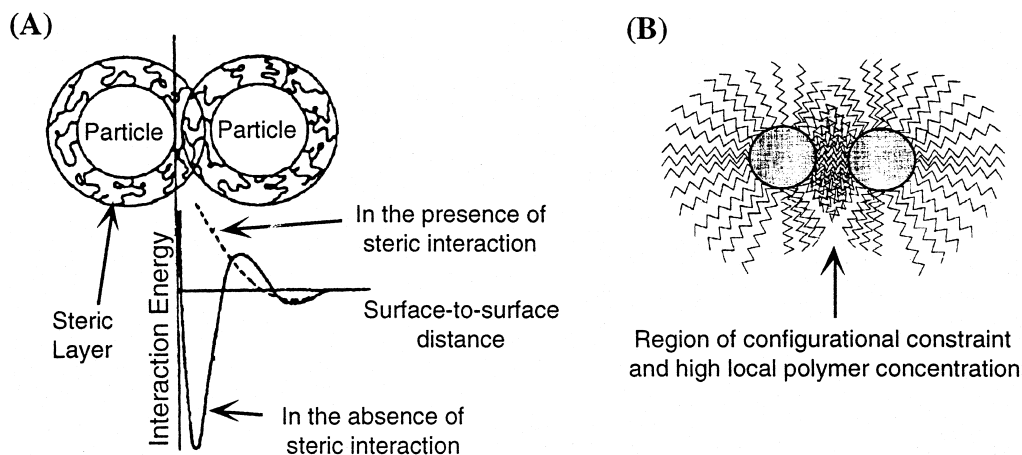

Fig. 2. (A) Schematic image of steric stabilization by adsorption of polymer chains onto a nanoparticle in solution [58]. The steric layer created by the adsorbed polymers presents a large barrier against particle interaction, thus slowing aggregation. (B) The inset to the right presents a close-up image of two polymer-protected particles interacting. The region between the two particles becomes crowded as a high local concentration of polymer builds up [2].
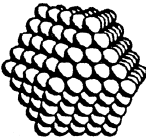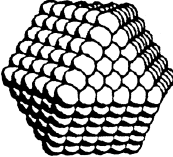
Full-Shell "Magic Number" Clusters					
Number of shells	1	2	3	4	5
Number of atoms in cluster	M_{13}	M_{55}	M_{147}	M_{309}	M_{561}
Percentage surface atoms	92%	76%	63%	52%	45%

Fig. 3. Idealized representation of hexagonal close-packed full-shell 'magic number' clusters [60]. Each metal atom has the maximum number of nearest neighbors, which imparts some degree of extra stability to full-shell clusters. Note that as the number of atoms increases, the percentage of surface atoms decreases.

long-range ordering [62]. (Crystal structures of small, semiconductor-type nanoclusters, notably $Cd_{32}S_{14}(SR')_{36}$, have been published, however [63].) One definition of the related colloid state is, of course, that it is a state that *cannot* be crystallized.

As an aside, one might argue that the development of the necessary characterization techniques in materials chemistry—primarily transmission electron microscopy—proved crucial to the rapid progress of ligand-stabilized nanocluster chemistry in the past decade. Despite such advances, determining the structure and composition of nanoclusters, and in particular determining the exact structure and bonding of the interaction between the metal surface and stabilizing 'ligands', is still a daunting task.

2.4.1. Transmission electron microscopy

The most widely used technique for characterizing nanoclusters is transmission electron microscopy (TEM) or high resolution TEM (HR-TEM), techniques which provide direct visual information on the size, shape, dispersity, structure, and morphology of nanoclusters [64]. (TEM is capable of routine magnifications of $\geq 400,000$, to, typically, a ± 2 Å resolution.) Potential draw-
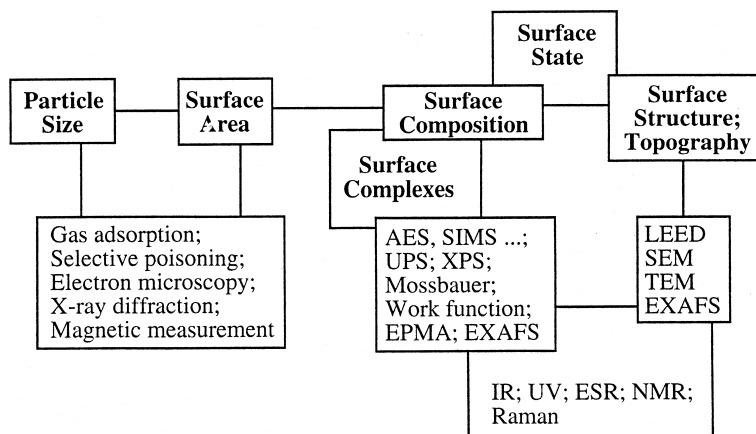
Fig. 4. Common methods available for the characterization of nanoclusters, adapted from Ref. [61].

backs of this technique include (i) the many reported examples of electron-beam-induced nanocluster structural rearrangement, aggregation, or decomposition; [3] (ii) the inherent problems in interpreting two-dimensional images of three-dimensional samples [64]; (iii) the small sample sizes, meaning that only a finite number of nanoclusters may be examined and counted, which may not be representative of the sample as a whole [64] (and, in any event, are often only 10^{-22} or so of Avagadro's number!); and (iv) the fact that samples must be dried and examined under high-vacuum condition, meaning that no direct information is gained on how the nanoclusters exist *in solution*. Despite these potential limitations, TEM has arisen as the technique of choice for the initial characterization of nanoclusters due to the atomic-level resolution possible, the speed of analysis, and the powerful visual images that are obtained.

2.4.2. UV–Visible spectroscopy (UV–Vis)

UV–Vis spectroscopy is particularly effective in characterizing semiconductor-type nanoparticles or metal particles whose plasmon resonance lies in the visible range—such as Cu, Ag and Au (for a compilation of the absorption spectra of several colloidal metallic elements see Ref. [70]). UV–Vis has also been used to determine both particle size and the degree of cluster aggregation in the sample. For example, Chestnoy et al. demonstrated the correlation between a *semiconductor* nanoparticle's size and its UV–Vis spectrum in 1986 [71]. As the particle size decreases, the λ_{max} shifts to shorter wavelengths, due to the band gap increase of the smaller-sized particles [26,30]. Wilcoxon et al. show that the optical spectra of semiconductor nanoclusters (MoS_2) are sensitive to the size and shape of the clusters, the amount of aggregation in the sample, the surface structure, and the presence of any adsorbates [26].

For transition metal nanoclusters, few in-depth studies have been published which correlate UV–Vis spectra to particle size. (Reetz's UV–Vis characterization of 14 Å, 23 Å, and 41 Å ($n\text{-}C_8H_{17})_4N^+Br^-$-stabilized Pd nanoclusters is one such example, however [72].) There is a wealth of UV–Vis spectra for colloidal metals (i.e., particles $\geq$ ca. 100 Å in diameter), as larger-sized particles can be more easily treated by theory, for example Mie Theory [73]. For colloidal particles which have an absorption band in the visible region, the λ_{max} is dependent on the size and the shape of the particles, as well as how close the particles are relative to each other [73]. Hence, not only can a particle's size be determined by UV–Vis spectroscopy, but phenomena such as aggregation can also be studied. In cases where the surface plasmon resonance can be identified, changes in surface *composition* can also be followed [74]. The ability to *tune* the optical properties of a system by changing particle size, degree of aggregation, or surface composition holds potential for many applications. For instance, Mirkin et al. have reported a reversible, colorimetric (red → blue), sequence-specific polynucleotide detection method based on aggregating mercaptoalkyloligonucleotide-modified 130 Å gold nanoparticles [9].

2.4.3. Infrared spectroscopy and surface enhanced Raman spectroscopy

Infrared spectroscopy (IR) has been used as a surface probe in nanocluster systems, commonly done by adsorbing carbon monoxide onto the surface of the metal nanocluster. Carbon monoxide is an ideal ligand because it readily adsorbs to metal surfaces, and has characteristic vibrational frequencies around 1800–2100 cm^{-1} once adsorbed or coordinated to the metal surface [2].

---

[3] For the aggregation of Au clusters under the electron beam of a TEM see Ref. [65]. For an account where the stabilizing ligand shell is lost and the Au nuclei rearrange see Ref. [66]. For observation of mobile surface atoms see Ref. [67]. For individual crystallite aggregation see Ref. [68]. For loss of ligands, and reduction and relaxation of the metal core, see Ref. [69]. See also Ref. 18 elsewhere [15].

Lewis and Lewis provided an early report of CO adsorbed to suspended metal particles, showing linear and doubly-bridging CO (at 2050 and 1880 cm^{-1}, respectively) on 23 Å Pt particles in methylene chloride [17]. However, Bradley has published the most comprehensive work in this area by reporting numerous IR studies of CO adsorbed onto colloidal and nanocluster metal surfaces [75–82]. He demonstrated that the infrared spectra of metal-bound CO changes drastically as the size of the metal particle changes [75–82]. For instance, a systematic IR study, of saturating CO adsorption of poly(vinyl pyrrolidone)-stabilized Pd clusters with diameters of 25 Å, 40 Å, and 60 Å in methanol, showed that as the Pd particle size increased, the ratio of terminal CO to bridging CO *decreased* [76]. Moreover, the largest particles (60 Å) showed *only bridging CO* on the metal surface. He attributes this change a result of a geometry change: as the size of the nanocluster increases, the number of edge sites (where linear CO is more stable), compared to face sites (where bridged CO is more stable), decreases [76]. Bradley has also used CO as a probe to study metal-surface enrichment in bimetallic Cu/Pd nanoclusters [77]; he finds that CO binds to both Cu and Pd, indicating that both metals are at the surface of the nanoparticles. Others have studied the effect of pH on nanocluster surface-bound CO [83], finding that increasing the pH leads to reduced CO coverage on Pt nanoparticles.

To a lesser extent, Surface Enhanced Raman Spectroscopy (SERS) has been used to probe the surfaces of small metal particles, often by following the absorption of pyridine on gold and silver sols [84]. (Pyridine as an adsorbate is known to initiate nanocluster agglomeration [2]). SERS has also been used to follow adsorbed molecules or ions formed during cluster synthesis (i.e., adsorbed citrate during aqueous Fe(II) reduction of Ag(I) [85]). The drawback of SERS is that its use is limited to metals which have a well-defined plasmon band [86] needed to provide the required signal enhancement.

2.4.4. Nuclear magnetic resonance

There are two uses for nuclear magnetic resonance (NMR) spectroscopy of nanoclusters: studies probing the intra-core metallic atoms, and studies probing the ligands that surround the metal core. The most revealing work has been in the latter area, which will be discussed in a moment in the context of various case studies, [4] for example, the ^{31}P NMR data on a $Rh_{\sim 55}(PPh_3)_{\sim 12}Cl_{\sim 6}$ nanocluster [89].

NMR studies of the metallic core (i.e., ^{105}Pd or ^{195}Pt NMR) are typically more difficult. This is because the nuclear-spin lattice relaxation time, and the nuclear resonance frequency itself, are sensitive to any metallic property the cluster may exhibit [90]. This change in frequency is known as the Knight shift [90], and is a consequence of the interaction of the metal nucleus with the conduction electrons [2,3]. (The largest Knight shift observed is −3.5% for ^{195}Pt, which corresponds to 35,000 ppm [91].) In very small particles and in favorable cases, the Knight shift allows resonances for surface and interior metal particles to be identified [91].

2.4.5. Scanning Tunneling Microscopy (STM) and Atomic Force Microscopy (AFM)

Scanning Tunneling Microscopy [92] makes possible the determination of the *total diameter of a nanocluster, including the stabilizing ligand shell*. STM is also an effective probe of the electronic properties of such nanoparticles. [5]

---

[4] For two examples not discussed in Section 3 (i.e., NMR studies of alkylthiols adsorbed on Au nanoparticles), see Refs. [87,88].

[5] For example, see Ref. [93], where the authors determine the double tunnel junction potential, or so-called 'Coulomb staircase', on several small metallic particles. See also Ref. [94]. For STM studies of some *polyoxoanions*, including $[PW_{12}O_{40}]^{3-}$, $[Cu_4(H_2O)_2(P_2W_{15}O_{56})_2]^{16-}$, $[P_2Mo_{17}VO_{62}]^{7-}$, and $[NaP_5W_{30}O_{110}]^{14-}$, see Ref. [95].

Early STM investigations of ligand-stabilized nanoparticles were not conclusive [6] [96], but in 1991 Schmid et al. published the first STM images of his phosphine-stabilized $Au_{\sim 55}[(C_6H_5)_3P]_{\sim 12}Cl_{\sim 6}$ and $Au_{\sim 55}[(C_6H_5)_2PC_6H_4SO_3Na]_{\sim 12}Cl_{\sim 6}$ clusters where the ligand shell was clearly visible [97]. Although the resolution of the metal core was not as good as anticipated [7] [97,98], Schmid found that the overall diameter of the clusters *including the ligand shell* was 22 Å, in good agreement with the expected diameter of 20–24 Å.

In 1994, Reetz et al. published a combined STM/TEM study of $R_4N^+Br^-$-stabilized Pd nanoclusters. He was able to determine the thickness of the stabilizing ligand shell by subtracting the STM-determined diameter from the TEM-determined diameter [99]. Reetz et al. found that the thickness of the stabilizing $R_4N^+Br^-$ layer was in good agreement with theoretical models [99]. However, tip effects must be considered [100], and Schmid and Peschel have shown that this technique may overestimate a particle's diameter, particularly when individual particles are imaged (vide infra) [101].

Despite the recent advances, STM remains an under-utilized nanocluster characterization technique. The drawbacks of STM include: (i) the nanoparticles tend not to stick well to the substrate surface, preventing good images from being obtained; (ii) the geometry of the tip shape may lead to inaccurate measurements or artifacts in the image; (iii) the tunneling mechanism is not well understood [99]; (iv) the samples examined are often dried solids, and hence no rigorously logical conclusions can be made about what the nanoclusters look like *in solution*; and finally (v) the specific techniques applied to image nanoclusters are far from mature, so that standard literature protocols have not been established.

Others have used atomic force microscopy (AFM) to image nanoclusters [100]. This technique, contrary to STM, is purely mechanical: a cantilevered tip attached to a spring is dragged across a sample. The increase or decrease in the height of the tip is measured, yielding a surface height profile as a function of distance. The advantage of this technique, relative to STM, is that it can be carried out on *nonconducting* samples. In a study of 30–160 Å gold particles in which the identical particles were imaged by both AFM and TEM, Giersig found that the AFM can reliably determine a particle's height, but is poor at determining its diameter [100]. Likewise, AFM cannot distinguish between subtle shape differences, or image particles that are spatially close to each other [100].

In a more recent combination STM/AFM study, in which pellets and monolayers of ligand-stabilized clusters and colloids were imaged by STM and AFM, the authors demonstrate that the combination of tip geometry and surface effects (in both the STM and AFM) *can lead to broadened images of spherical particles* [101]. This results in an overestimation of particle size, an effect that is more pronounced in STM compared to AFM studies.

---

[6] One of the first reports using STM to investigate ligand stabilized nanoclusters was van Kempen et al.'s images of $Pd_{\sim 561}(phen)_{\sim 38 \pm 2}O_n$ and $Au_{\sim 55}(PPh_3)_{\sim 12}Cl_{\sim 6}$. They found that the observed height of $Pd_{\sim 561}(phen)_{\sim 38 \pm 2}O_n$ clusters ($\sim 15 \pm 3$ Å) did not match the calculated value of at least 24 Å (for the metal core alone), and concluded that the ligands could not be observed unequivocally under the conditions of the experiment. Furthermore, they observe that (i) features were present that show that the clusters were being picked up, brushed aside, and dragged around by the probe tip; and (ii) the clusters seemed to aggregate around the steps in the highly oriented pyrolitic graphite (the substrate), indicating that the steps were probably 'arresting diffusion' of the clusters. Furthermore, when van Kempen examined $Au_{\sim 55}(PPh_3)_{\sim 12}Cl_{\sim 6}$, he found that single clusters could not be resolved. Instead, the gold clusters aggregated into larger clusters with heights as large as 100 Å [96].

[7] It is believed that the organic ligand shell blurs the substructure of the gold core. This is in contrast to Wang's STM study of polymer-protected 25 Å Rh and 40 Å Au colloids, where the arrangement of the metal atoms could be observed (they were irregular, however, and not the expected ccp structure) but the stabilizing polymers could not be seen [98]. Nevertheless, although Schmid's STM images were clearly different than those of *non-stabilized* metal clusters, he could not distinguish between the $[(C_6H_5)_3P]_{12}Cl_6$- or $[(C_6H_5)_2PC_6H_4SO_3Na]_{12}Cl_6$-stabilized clusters in the STM.

3. Part Two. Five important case studies in nanocluster chemistry

To provide an overall perspective of nanocluster chemistry, five Case Studies are presented below. Each Case Study discusses the work of a specific research group. Despite the varying chemistry, methodology, and applications of nanoclusters in each study, several themes become apparent. For instance, each group synthesizes transition metal nanoclusters in non-aqueous solvents, each utilizes a common set of characterization techniques, and each investigates the nanoclusters for their catalytic activity.

Table 1 provides an overview of each of the Case Studies. The first one presented is the work of Schmid et al. who synthesized the seminal $Au_{55}(PPh_3)_{12}Cl_6$ cluster. Next, the work of Moiseev et al. is discussed, the first to successfully use nanoclusters as catalysts *in solution*. Bönnemann et al.'s nanocluster syntheses utilizing dual reducing/stabilizing agents is then considered, followed by an examination of Reetz et al.'s elegant electrochemical syntheses and characterization studies of $NR_4^+X^-$ stabilized metal clusters. Finally, the case of polyoxoanion- and tetrabutylammonium-stabilized transition metal nanoclusters is presented and discussed.

3.1. Case I. Schmid's $Au_{55}(PPh_3)_{12}Cl_6$ ligand-stabilized cluster: the first example of a well-defined ligand-stabilized nanocluster

3.1.1. Synthesis

Günter Schmid et al. at the University of Essen, Germany, established the field of ligand-stabilized transition metal nanoclusters with the synthesis of $Au_{55}(PPh_3)_{12}Cl_6$ in 1981 [102]. Since that time, their work has taken them from the synthesis and characterization of nano-sized clusters, to the investigation of the discrete metal/bulk metal interface through the utilization of transition metal nanoclusters as heterogeneous catalysts.

An important cluster synthesized by Schmid is the 'magic number' (i.e., M_{55}) [60] 14 Å $Au_{55}(PPh_3)_{12}Cl_6$ complex. This molecule is made by passing diborane, B_2H_6, through a 50–60°C benzene solution of PPh_3AuCl. The diborane reduces Au(I) to Au(0) and complexes excess phosphine [89]. A black solid is isolated which has an analytical formula of $[Au_{9.2}(PPh_3)_2Cl]_n$; sedimentation molecular weight measurements give a molecular formula approximately 6-fold larger, or $Au_{\sim 55}(PPh_3)_{\sim 12}Cl_{\sim 6}$ [102]. The chief disadvantage of this procedure is that Au(0) metal is produced as an unwanted by-product. Also, the resulting nanoclusters have a limited thermal stability, decomposing in solution when warmed to 50–60°C [102]. The diborane-as-reductant route has been extended to other metals, leading to the synthesis of clusters with the general formula $M_{55}L_{12}Cl_x$ where M = Au, Rh, L = PPh_3, $x = 6$; M = Rh, Ru, L = $P(t$-Bu$)_3$, $x = 20$; M = Pt, L = $As(t$-Bu$)_3$, $x = 20$; M = Co, L = PMe_3 $x = 20$ [89,103].

The proposed structure of the $Au_{55}(PPh_3)_{12}Cl_6$ complex is shown in Fig. 5 and is based largely on Mössbauer spectroscopy [89,102]. (Attempts to grow crystals of this complex for X-ray crystallography were unsuccessful [89]). Mössbauer spectroscopy indicates that there are four different environments for the Au atoms, which Schmid et al. assign as (i) core Au atoms (13 atoms), (ii) uncoordinated surface Au atoms (24 atoms), (iii) phosphine-coordinated surface Au atoms (12 atoms), and (iv) chloride-coordinated Au surface atoms (6 atoms) [89,102]. This fits a model consisting of a two-shell cubic-close-packed Au metal core where twelve PPh_3 ligands occupy the twelve vertices and six chloride ligands sit on the square faces of the cubooctahedron [103].

Schmid also synthesized the air-stable, water-soluble, four-shell $Pt_{\sim 309}Phen^*_{\sim 36}O_{\sim 30 \pm 10}$ nanocluster (by the H_2 reduction of platinum(II) acetate in acetic acid, with approximately 30% yield), for

Table 1
The five literature nanocluster case studies presented in this review

Case	Who/Where	Nanocluster system(s)	Synthesis	Characterization	Catalysis	Significance	Refs.
Case I	Günter Schmid et al./Max Planck Institute, Mülheim	14 Å 'Au$_{55}$(PPh$_3$)$_{12}$Cl$_6$' and other M$_{55}$L$_{16}$Cl$_8$ systems; also 'Pt$_{309}$Phen$_{36}$O$_{30 \pm 10}$' and 'Pd$_{561}$Phen$_{36}$O$_{190-200}$'.	Diborane reduction of PPh$_3$AuCl in benzene.	TEM; HR-TEM; some STM; ^{31}P NMR; Mössbauer; Desorption and Secondary Ion Mass Spectrometry.	Heterogeneous catalysis: hydroformylation, hydrogenation, and hydrosilylation; studied reactivity of some bimetallic clusters.	One of the first examples of a ligand-stabilized nanocluster.	[101–111, 113–119, 121–131]
Case II	Ilya Moiseev et al./Academy of Sciences, Moscow	'Pd$_{561}$L$_{60}$(OAc)$_{180}$' [L = phen, bipy] and 'Pd$_{561}$phen$_{60}$O$_{60}$(PF$_6$)$_{60}$'.	Hydrogen reduction of Pd(II)acetate in acetic acid; workup under oxygen.	TEM; ^{1}H NMR; Elemental Analysis; Molecular Weight; EXAFS; SAXS.	Catalysis in solution: hydrogenation, dimerization, isomerization, oxidative acetylation and carbonylation; some reactions are inhibited by O$_2$. Proposed mechanism with nanocluster as catalyst.	First example of nanocluster catalysis once redispersed in solution; first proposed mechanism with nanocluster as catalyst.	[20,132–135] [136]
Case III	Helmut Bönnemann et al./Max Planck Institute, Mülheim	10–100 Å R$_4$N$^+$ X-stabilized nanoclusters of various transition metals; some solvent-stabilized (THF, thioethers) clusters.	Reduction of metal salts in THF by combined reducing and stabilizing agent, R$_4$N(BEt$_3$H).	TEM; HR-TEM; Elemental Analysis; EDS.	Heterogeneous-type catalysis: hydrogenation, enantioselective hydrogenations.	Wide range of metals studied; first enantioselective hydrogenations; extensive use as heterogeneous catalysts.	[16,19,57] [137,138] [139,140] [141,142] [143,144] [145,146] [147,148]

|						
Case IV	Manfred Reetz et al./Max Planck Institute, Mülheim	14–48 Å R_4N^+ X-stabilized Pd nanoclusters; some solvent-stabilized clusters (propylene carbonate) reported.	Size-selective control of particles via electrochemical synthesis in THF/CH_3CN solution	Combined TEM/STM study; EXAFS; UV–Vis; cyclic voltammetry.	Heterogeneous 'Cortex' catalysts: olefin hydrogenation and Heck reactions; Dispersed in solution: Heck and Suzuki coupling reactions.	Clean, large-scale synthesis; elegant characterization.	[12,21,22] [23,24,72] [99] [149,150] [151,152] [153,154] [157,158] [159,160] [161]
Case V	Richard Finke et al./Colorado State University	20 and 30 Å polyoxoanion- and tetrabutylammonium-stabilized $Ir(O)_{\sim 300}$ and $Ir(O)_{\sim 900}$ nanoclusters.	Reduction of polyoxoanion-supported organometallic complex in acetone under H_2.	TEM, HR-TEM; STM; UV–Vis, FAB-MS, Solution molecular weight, IR, Electron Diffraction, Ion-Exchange Chromatography	Isolated and redissolved $Ir(O)$ nanoclusters retain catalytic activity in cyclohexene hydrogenation; show up to 18,000 total turnovers.	First modern mechanistic and kinetic study of transition metal nanocluster nucleation and growth. Longest proven catalytic lifetime in solution. Unusual polyoxoanion stabilization.	[1,15,52] [162]

$$\mathbf{Au_{55}[P(C_4H_5)_3]_{12}Cl_6}$$
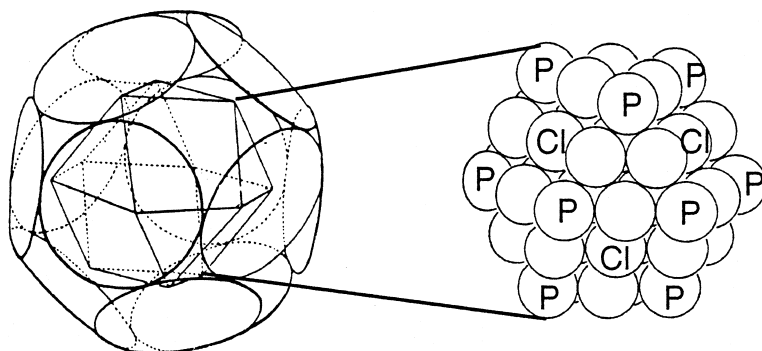
Fig. 5. Schmid's proposed structural model for the $Au_{55}(PPh_3)_{12}Cl_6$ ligand-stabilized nanocluster. The image on the left [89] contains the metal core (indicated by the internal cubooctahedral) surrounded by the phosphine ligand shell radii (indicated by the circles in the left-hand side image), while the inset on the right [103–105] shows the ccp Au_{55} metal core alone with the proposed phosphine and chloride ligand binding sites at each metal (labeled P and Cl, respectively).

which he obtained elemental analysis for all elements present [106], and the related $Pd_{\sim 561}$-$Phen_{\sim 36}O_{\sim 190-200}$ nanocluster [103]. The phenanthroline- and phenanthroline*-stabilized nanoclusters are more thermally robust than their phosphine stabilized counterparts. Both are sensitive to added electrolyte.

One interesting feature of the organic-solvent-soluble $Au_{55}(PPh_3)_{12}Cl_6$ complex is that it can be made water-soluble by exchanging the PPh_3 ligands with hydrophilic derivatives such as $Ph_2PC_6H_4SO_3Na \cdot 2H_2O$ [107,103]. Conductivity measurements indicate that the water soluble complex dissociates into 12 Na^+ and $[Au_{55}(L)_{12}Cl_6]^{12-}$ in solution; the diffusion coefficient of this cluster is measured to be approximately 1.5×10^{-10} m^2 s^{-1} [108].

3.1.2. Characterization

Schmid and co-workers characterized their clusters by a multitude of techniques, both to investigate their structure and to answer the quintessential question: ''How small does a metal particle have to be so that bulk properties like conductivity, magnetism, etc., begin to disappear . . . ?'' [109].

3.1.2.1. The structural issue.
Schmid published some of the most impressive TEM and HR-TEM images of nanoclusters that exist, including images that clearly show a metal core surrounded by a stabilizing ligand shell (Fig. 6) [109]. But despite such beautiful images, Schmid finds that the electron beam of the TEM often causes metal atom rearrangements, cluster growth, and ligand desorption from the metal surface [109].

Schmid was the first to study ligand-stabilized nanoclusters by STM [110], albeit with mixed success, studies which highlight the difficulties in obtaining meaningful STM images on clusters of this type. STM measurements of the $Au_{55}(PPh_3)_{12}Cl_6$ cluster show a total diameter of 21–25 Å (vs. ca. 14 Å for the metal core alone, by TEM), in expected agreement with theoretical predictions [97]. However, Schmid was one of the first to recognize the problems inherent in measuring cluster diameter by STM. For instance, the clusters can aggregate [110,111], stick to the STM probe tip [112], move about on the substrate surface, appear to flatten out, fragment, appear 'floppy', or be pulled into the substrate surface. However, his work led to improvements in the imaging of nanoclusters [97,113], and opened the door for Reetz's STM experiments described later in this review.

Fig. 6. Left, HR-TEM image of a 132×105 Å gold colloid surrounded by two layers of $P(m\text{-}C_6H_4SO_3Na)_3$ stabilizing ligands. Right, HR-TEM image of a Pt_{309} cluster molecule in the (110) direction showing nine rows of the fcc structure, corresponding to a four-shell cluster. Both images are from Ref. [109].

Perhaps Schmid's most interesting characterization results are his proton decoupled ^{31}P NMR data on the $Rh_{55}(PPh_3)_{12}Cl_6$ nanocluster [89,114]. This spectrum shows a singlet with no ^{31}P–^{103}Rh coupling in both acetone and CH_2Cl_2 at room temperature; no additional peaks are seen when excess phosphine is added, but the signal moves to higher field. Schmid concludes that there is fast exchange between the free and nanocluster-bound phosphine ligands, and calculates an average phosphine binding time to the cluster surface of 3.0 ± 0.5 μs [89]. The ^{31}P NMR *in pyridine*, however, shows an additional peak attributed to *free* phosphine. From this, he concludes that the more coordinating solvent pyridine *displaces* phosphine ligands from the metal surface. Recall that pyridine is the ligand commonly used to cause agglomeration of nanoclusters and nanocolloids [2].

An enlightening series of experiments using ^{252}Cf plasma desorption mass spectrometry [163], secondary ion mass spectrometry (the first use of mass spectrometry to characterize such molecules) [164], and angle-resolved X-ray photoelectron spectroscopy [165] caused a reexamination of how we are to consider such molecules: well-defined and discrete, or an *ensemble* of particle sizes and compositions?

Despite the early use of precise stoichiometries such as '$\mathbf{Au_{55}}(PPh_3)_{12}Cl_6$', '$\mathbf{Pt_{309}}Phen^*_{36}O_{30 \pm 10}$', and '$\mathbf{Pd_{561}}Phen_{36}O_{200}$' (note that each is *formulated* as a magic number), the $Au_{55}(PPh_3)_{12}Cl_6$ cluster is reformulated by others—after some controversy, it appears [166]—as "$Au_{67}(PPh_3)_{14}Cl_8$ with smaller clusters as impurities" [163]. It is now agreed that "ligand stabilized colloids cannot be regarded as stoichiometrically well-defined molecules" [115], particularly since mass spectrometry of several identically-prepared samples of $Au_{55}(PPh_3)_{12}Cl_6$ in different laboratories gave conflicting results. Ultimately, it was concluded that (i) samples of $Au_{55}(PPh_3)_{12}Cl_6$ prepared in different laboratories give different spectra *and are different*; (ii) the clusters change with time, and that during the aging process the samples become inhomogeneous; (iii) the mass spectrum of the clusters depends on the source, the age, and the storage history of the sample; and (iv) neither a full-shell, 'magic number' structure nor an alternatively-proposed vertex-sharing icosahedral structure could be confirmed [166]. This example demonstrates the power of mass spectrometry in nanocluster science, and argues for its use in every applicable case.

Angle-resolved X-ray photoelectron spectroscopy supports the conclusion that samples of '$Au_{55}(PPh_3)_{12}Cl_6$' contain gold species that differ from the $Au_{55}(PPh_3)_{12}Cl_6$ formulation: in a study of ten individual $Au_{55}(PPh_3)_{12}Cl_6$ samples examined by XPS, four agreed with the '$Au_{55}(PPh_3)_{12}Cl_6$' formulation (although two of these four showed the presence of larger particles), while the remaining

six showed a distribution of particle sizes, in addition to discrete, single-metal-atom Au(I) species [165].

We will use $Pd_{\sim 561}$ as a *useful shorthand nomenclature*, one first presented elsewhere [15], to designate a distribution of nanoclusters that center about, for example, a 'Pd_{561}' magic number cluster. It must be emphasized, however, that this is just a useful shorthand for the *distribution of nanoclusters present*; nothing approaching truly monodisperse is indicated, nor present, in '$Pd_{\sim 561}$'.

3.1.2.2. When do bulk metal properties disappear? Schmid finds that even metal clusters as small as 15 Å have some bulk metal characteristics [60,116–119] and concludes that ''the formation of a metallic state is mainly determined by the cluster nucleus, and not by the surface atoms'' [109]. Magnetic measurements show that the $Au_{\sim 55}(PPh_3)_{\sim 12}Cl_{\sim 6}$ metal core displays a small amount of bulk metal character, and Schmid writes that this molecule should be considered 'more as a molecular colloid of gold' [118]. In addition, SQUID measurements on the $Pd_{\sim 561}$ cluster show that the inner $Pd_{\sim 309}$ core shows bulk-metal-like magnetic susceptibility [120], λ, while the outer layer does not, presumably due to signal attenuation by the presence of the ligand shell [109]. The ^{195}Pt NMR of $Pt_{\sim 309}$ clusters is also consistent with this conclusion: two relaxation times are measured, one due to inner-shell (metal-like) and one to outer-shell (non-metal-like) Pt atoms [109]. Finally, measurements of electronic energy relaxation in Au clusters indicate that the transition between bulk and molecular-type species occurs between 55 and 13 atoms [121].

3.1.3. Catalysis and other uses

In his early hydrogenation and hydroformylation attempts with Rh clusters *in solution*, Schmid found that the original cluster decomposed and was not retained after the reaction [119]. Believing at the time that ''the application of large clusters [as catalysts] can only be done via the formation of heterogeneous catalysts'' [122], Schmid turned his attention to supported nanocluster heterogeneous catalysts [123]. He found that two conditions are needed to make heterogeneous catalysts from transition metal nanoclusters: first, the nanoclusters must have neutral ligand stabilizers (i.e., they *must not contain ionic groups*), and second, the solid support must contain micropores (i.e., it cannot have a smooth surface) [109]. These conclusions are, however, preliminary ones that require additional testing since, for example, Reetz's so-called 'cortex' catalysts are designed to put the nanocluster on the *surface* of a solid support rather in its micropores (vide infra).

Schmid studied monometallic clusters as heterogeneous catalysts, finding that Rh and Pd clusters on TiO_2 and Al_2O_3 are effective hydroformylation [109] and hydrogenation catalysts [124]. The nature of the stabilizing ligand shell has a significant effect on both selectivity and activity in the hydrogenation of hex-2-yne by Pd nanoclusters [124].

In his study of bimetallic Au/Pd clusters grown by his 'seed-growth' method (Au core, Pd outer shell, Fig. 7), and supported on TiO_2 for the heterogeneous hydrogenation of hex-2-yne, Schmid shows that the gold core *increases* the catalytic activity of the Pd shell; he also finds, as one might expect, that the influence of the Au core increases as the thickness of the outer Pd shell *decreases* [125].

In a study of bimetallic Au/Pd, Au/Pt, and Pd/Pt clusters supported on Al_2O_3 in hydrosilylation reactions [115], the catalytic activity was found to decrease in the trend

$$Pd/Pt \approx Pt > Au/Pt \gg Pd, Au.$$

The authors report TEM images which show a Pd core surrounded by a darker Pt outer shell. These supported clusters exhibit good lifetimes, showing a constant catalytic activity over at least six cycles
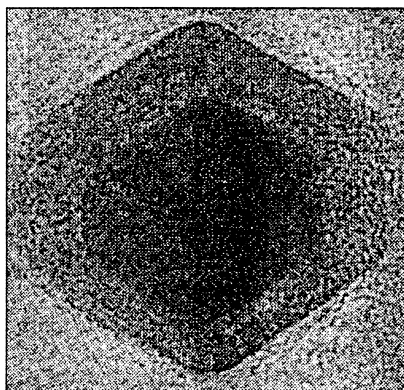
Fig. 7. HR-TEM image of a bimetallic, monocrystalline Au/Pd cluster. EDX analysis shows that the inner core is Au while the outer layer is Pd [109].

of reuse [123]. In contrast, TEM images of the bimetallic Au/Pt clusters show a homogeneous Au inner core surrounded by *individual Pt particles*, and not a smooth shell layer, for reasons that Schmid notes are 'not completely understood' [109]. Heterogeneous catalysis with these clusters began after an induction period (attributed to the time needed to remove O_2 from the surface of the cluster, present from workup under air). The thinner the outer Pt coating, the more active the supported Au/Pt clusters are in hydrosilylation catalysis [115]; furthermore, this catalyst becomes deactivated after one cycle at 120°C but retains 70% of its original activity after 4 cycles at 60°C.

The syntheses of bimetallic nanoparticles of two metals (M_1 and M_2), of known initial structure (i.e., one metal at the core, a second metal on the surface), appear to be possible by the seed-growth method [115] (i.e., the living metal polymer [167] method); characterization by EDX [168], optical absorption spectroscopy [168], EXAFS [169], and HR-TEM [168] has been reported (see elsewhere [169], however, for a discussion of some of the issues in using EXAFS to characterize bimetallic nanoclusters). Many issues remain in this area, such as: the relative stabilities of $M_{1(core)}/M_{2(surface)}$ vs. $M_{2(core)}/M_{1(surface)}$ nanoclusters [115], which metal(s) are actually doing the catalysis, whether or not imperfections in the nanoclusters are involved in catalysis (i.e. where the ostensibly core metal might be somewhat on the surface or otherwise exposed to the substrate), and so on. Hence, additional studies of bimetallic and higher multimetallic nanoclusters can be anticipated in search of improved catalytic selectivities, activities, and lifetimes.

Finally, Schmid has joined others (vide infra) in attempting to order his clusters into long-range molecular assemblies [126–129], with the ultimate aim of creating molecular-scale devices. By dipping a poly(ethyleneimine)-coated mica substrate into an aqueous solution of Au_{55} clusters, Schmid creates a two-dimensional Au cluster array that contains less than 5% surface disorder [130], Fig. 8. Schmid et al. have also grown rudimentary wires from Au clusters and colloids in the pore channels of alumina membranes [131].

3.2. Case II. Moiseev's giant palladium clusters. The first example of nanocluster catalysis in solution

One of the most-studied catalytic nanocluster systems in the literature is Moiseev et al.'s giant cationic palladium clusters, with the *approximate* formulas $Pd_{\sim 561}L_{\sim 60}(OAc)_{\sim 180}$ [L = 1,10-phenanthroline or 2,2′-bipyridine] and $Pd_{\sim 561}phen_{\sim 60}O_{\sim 60}(PF_6)_{\sim 60}$. These clusters have been extensively characterized, and were the first example of isolable nanoclusters that did catalysis while
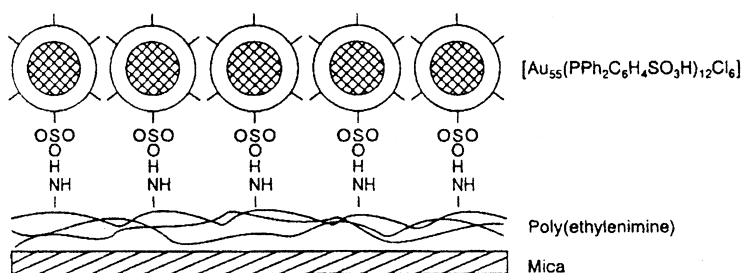
Fig. 8. Schematic illustration, taken from Ref. [130], of the array created by depositing Au_{55} clusters on a mica platelet (ca. 1 cm^2) coated with poly(ethylenimine). The platelet was immersed in a 3×10^{-6} M aqueous cluster solution for 24 h.

dispersed *in solution*; their exact compositions and overall charges are, however, still not known with certainty.

3.2.1. Synthesis and characterization

The 'large cluster' $Pd_{\sim 561}L_{\sim 60}(OAc)_{\sim 180}$ [L = phenanthroline, bipyridine] is formed in two steps. The first step is reduction of palladium(II) acetate by hydrogen in acetic acid, in the presence of either 1,10-phenanthroline (phen) or 2,2′-bipyridine (bipy) to yield an intermediate characterized as $[Pd_4phen(OAc)_2H_4]_n$ ($n \approx 100$). The overall stoichiometry of this reaction is given by Eq. (1) [20,132].

$$4Pd_3(OCOCH_3)_6 + 3\,phen + 15H_2 \rightarrow 3Pd_4phen(OCOCH_3)_2H_4 + 18CH_3COOH \qquad (1)$$
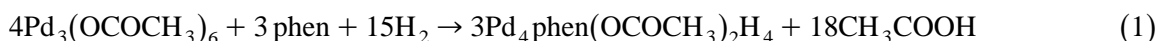
TEM images of $[Pd_4phen(OAc)_2H_4]_n$ ($n \approx 100$) show 20 ± 5 Å particles, a size supported by small angle X-ray scattering (SAXS) analysis [132]. (From this diameter, and assuming that the packing density of palladium is the same as in the bulk metal, the authors estimate n in the idealized formula as about 100, that is $Pd_{\sim 400}$.)

One of the few NMR studies in the literature between the interaction of the stabilizing ligand and the metal surface has been done on the $[Pd_4phen(OAc)_2H_4]_n$ ($n \approx 100$) nanocluster. The ^{1}H NMR spectrum in CD_3CN and CD_3OD of $[Pd_4phen(OAc)_2H_4]_n$ shows three types of resonances: (a) a broad resonance that spans -20 and -60 ppm; (b) a broadened, unresolved resonance between 6 and 9 ppm; and (c) a narrow and completely resolved resonance at 2 ppm [20]. Moiseev assigns the broad resonance centering at approximately -33 ppm to the hydrides, the unresolved resonance between 6 and 9 ppm to the phenanthroline group protons, and the resonance at 2 ppm to the protons in the $CH_3CO_2^-$ anion protons. He concludes that the considerable broadening of the hydride and phenanthroline resonances, Fig. 9, demonstrates that these ligands are coordinated *directly to the surface of the palladium cluster*, whereas the narrow resonance of the acetate anions suggest that they are not associated directly with the surface of the cluster while in solution.

Workup of $[Pd_4phen(OAc)_2H_4]_n$ ($n \approx 100$) in acetic acid, under oxygen, leads to the uptake of 0.5 mol of O_2 per gram-atom of palladium within 20 min. Subsequent washing with benzene and vacuum drying leads to the air-stable cluster characterized as $[Pd_9phen(OAc)_3]_{60}$ (or $Pd_{\sim 540}phen_{\sim 60}(OAc)_{\sim 180}$) in 85% yield. The molecular formula of this water- (and polar organic solvent-) soluble complex was established by elemental analysis, sedimentation–ultracentrifugation molecular weight, TEM [20], and SAXS [132].

TEM images of $Pd_{\sim 540}phen_{\sim 60}(OAc)_{\sim 180}$ show the presence of 26 ± 3.5 Å spherical particles, while SAXS (20 ± 5 Å) and electron diffraction (~ 25 Å) confirm the indicated size [132]. Although electron diffraction also confirms that the interplanar distances in this cluster match those in fcc bulk
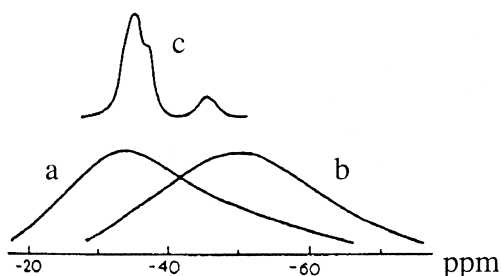
Fig. 9. The hydride region of the ^{1}H NMR spectrum of $[Pd_4L(OAc)_2H_4]_n$ ($n \approx 100$) showing broadened resonances, attributed to surface hydrides on the surface of the cluster [20]. (a) Solution of $[Pd_4L(OAc)_2H_4]_n$ ($n \approx 100$) where L = phenanthroline (b) L = bipy (c) magic-angle-spinning ^{1}H NMR spectrum of the solid.

palladium, EXAFS *conflicts with this* by showing an icosahedral packing order of the metal atoms in this same $Pd_{\sim 540}$ nanocluster. The authors attribute this disagreement to the high-energy electron beam of the TEM (the conditions under which electron diffraction is measured), conditions which appear to cause the packing structure of the metal atoms to rearrange from icosahedral to fcc [132].

Moiseev approximates the total number of atoms per cluster to be approximately 570. This value, combined with the elemental analysis and the solution molecular weight analysis, leads to the molecular formula $Pd_{570 \pm 30}phen_{63 \pm 3}(OAc)_{190 \pm 10}$, which is in close agreement to an idealized five-shell icosahedrally packed full-shell cluster ($n = 561$). Hence, Moiseev proposes an *idealized* formula of '$Pd_{561}phen_{60}(OAc)_{180}$', which in his words, ''seems to correspond to some average size and composition of [the] cluster, rather than to a certain fixed size and composition'' [132].

The $Pd_{\sim 561}phen_{\sim 60}(OAc)_{\sim 180}$ model is shown in Fig. 10. This model consists of the close-packed Pd-metal core surrounded by bulky phenanthroline ligands. In agreement with the molecular formula, the authors calculate that, geometrically, approximately 60 phenanthroline ligands can be coordinated
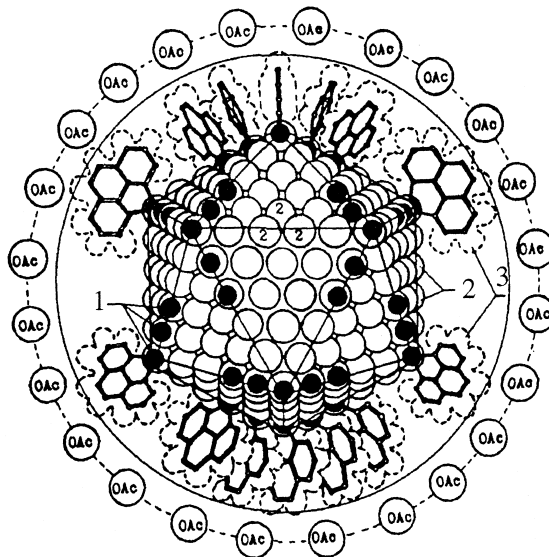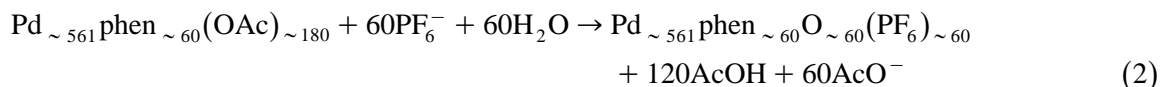

Fig. 10. The idealized model of $Pd_{\sim 561}phen_{\sim 60}(OAc)_{\sim 180}$ [20]. 1: Pd atoms coordinated with phenanthroline ligands; 2: Pd atoms accessible for coordination with OAc^- anions or molecules of substrates or solvent; 3: van der Waals surface of coordinated phenanthroline ligands.

in a bidentate fashion to the cluster's 252 surface Pd atoms. (The estimated thickness of the ligand shell is ca. 4.1 Å, as visualized by HR-TEM [133]). There remains some metal surface that is not directly covered by the phenanthroline ligands, arising from the fact that, sterically, the phenanthroline ligands may bond to only the edges and vertices of the icosahedron. It is not known whether or not the unligated metal atoms are the catalytically active site(s).

Again, as we saw in Schmid's case, such precise models and molecular formulas fall short of an accurate representation of the clusters. For example, fractionation of the Pd cluster into benzene:acetonitrile solutions (of varying ratios) shows increasingly more polydisperse and disordered clusters [133,134]. Likewise, HR-TEM images and electron diffraction data of $Pd_{\sim 561}$ $phen_{\sim 60}(OAc)_{\sim 180}$ provide evidence that there are at least three kinds of metal cores present in the sample: (i) nearly perfect-packed fcc metal particles; (ii) icosahedral multiple-twinned particles; and (iii) pseudo-amorphous Pd particles with only short range ordering [133,135].

$Pd_{\sim 561}phen_{\sim 60}(OAc)_{\sim 180}$ can be converted into $Pd_{\sim 561}phen_{\sim 60}O_{\sim 60}(PF_6)_{\sim 60}$ via substitution of OAc^- by PF_6^- in aqueous solution, Eq. (2) [20].

$$Pd_{\sim 561}phen_{\sim 60}(OAc)_{\sim 180} + 60PF_6^- + 60H_2O \rightarrow Pd_{\sim 561}phen_{\sim 60}O_{\sim 60}(PF_6)_{\sim 60}$$
$$+ 120AcOH + 60AcO^- \qquad (2)$$

In order to maintain charge balance (i.e., replacement of 180 OAc^- anions with only 60 PF_6^- anions), O_2 is introduced slowly, coordinating as oxide, O^{2-}, ligands onto the outer surface of the $Pd_{\sim 561}phen_{\sim 60}O_{\sim 60}(PF_6)_{\sim 60}$ cluster (as postulated from EXAFS data). Moiseev proposes that the 60 oxygen atoms coordinate as bridging groups on the 20 faces of the icosahedron, Fig. 11, and supplies EXAFS data in support of his postulate [20].

3.2.2. Catalytic properties

The hydride $[Pd_4phen(OAc)_2H_4]_n$ ($n \approx 100$) cluster catalyzes several simple hydrogenation, dimerization, and isomerization reactions in solution with turnover frequencies that range from 0.3 h^{-1} for the dimerization of propylene to 15 h^{-1} for the hydrogenation of ethylene, and lifetimes of up to 10,000 turnovers (uncorrected for the number of exposed Pd atoms) [20]. These reactions are inhibited by the presence of oxygen [132].

The clusters $Pd_{\sim 561}phen_{\sim 60}(OAc)_{\sim 180}$ and $Pd_{\sim 561}phen_{\sim 60}O_{\sim 60}(PF_6)_{\sim 60}$ were also shown to catalyze the oxidative acetoxylation of several small organic substrates with high selectivities (95–98%) [20]. These two clusters convert ethylene into vinyl acetate, propylene into allyl acetate,
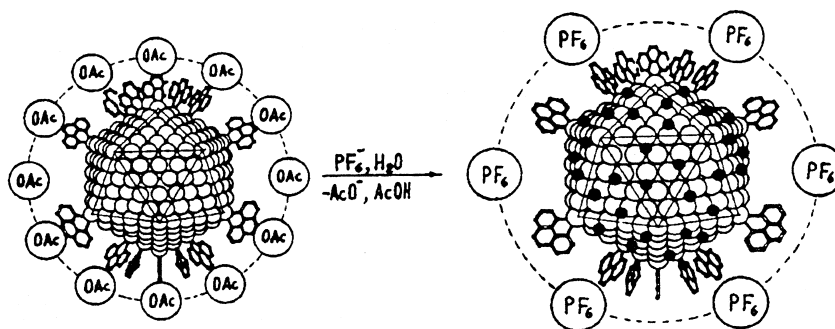

Fig. 11. A depiction of the substitution reaction of PF_6^- for OAc^- in the $Pd_{\sim 561}phen_{\sim 60}(OAc)_{\sim 180}$ cluster, leading to the formation of $Pd_{\sim 561}phen_{\sim 60}O_{\sim 60}(PF_6)_{\sim 60}$. The black circles represent the proposed location for the 60 oxygen atoms [20].

and toluene into benzyl acetate. Likewise, they oxidize primary alcohols into ethers, aldehydes, and acetals, and secondary alcohols into ketones [132], and have recently been shown to oxidatively carbonylate phenol to diphenyl carbonate, with the cluster serving as an electron-transfer mediator [136].

Moiseev studied the kinetics of ethylene and propylene oxidation by $Pd_{\sim 561}phen_{\sim 60}O_{\sim 60}(PF_6)_{\sim 60}$ in acetic acid/acetonitrile solutions (and in diglyme/acetic acid solutions) [20]. The proposed mechanism for ethylene oxidation by $Pd_{\sim 561}phen_{\sim 60}O_{\sim 60}(PF_6)_{\sim 60}$ nanoclusters is shown in Fig. 12.

The salient features of this proposed mechanism are as follows [20].

· Large poisons of metal active sites, such as PPh_3, show no effect on the observed catalytic rate, whereas small poisons, such as C_2H_5SH, suppress the catalytic activity of the cluster. (About 50 molecules of C_2H_5SH per cluster completely suppress the activity in ethylene oxidation, while only about 15 molecules of C_2H_5SH per cluster surface completely suppress propylene oxidation). These poisoning experiments indicate that for ethylene oxidation only about 20% of the surface Pd atoms are available as active sites, whereas for propylene oxidation only about 6% of the surface atoms are available as catalytic active sites. [8]

· Indirect evidence that the catalyst is *not* a mono-molecular Pd complex is provided by the lack of effect that small amounts of water have on product selectivity [as they expect when using a Pd(II) monomolecular complex]; indirect evidence that the catalyst is *not* bulk Pd metal is provided by kinetic isotope effects of $k_{C_nH_{2n}}/k_{C_nD_{2n}}$, which show a 3-fold difference between nanocluster-catalyzed ($k_H/k_D = 3.6 \pm 0.2$) and Pd-black catalyzed ($k_H/k_D = 1.0 \pm 0.1$) propylene oxidation.

· Kinetic isotope effects show that the k_H/k_D for ethylene is unity, whereas the k_H/k_D for propylene is 3.6 ± 0.2. These data suggest that in the ethylene case, the rate-determining step is oxidative addition of π-coordinated ethylene onto the Pd–Pd surface. In the propylene case, however, the rate-determining step is thought to be the breaking of an allyl–H bond to form a π–allyl complex and a surface hydride.

There is a need for additional studies of nanocluster-catalyzed reactions, especially on nanoclusters: (i) that are as well-defined as possible in their composition and size; (ii) that are undergoing more difficult, interesting reactions; (iii) where issues such as nanocluster fragmentation (to active species) are addressed; and (iv) where the nanocluster's mechanism is compared to that of traditional heterogeneous catalyst undergoing the identical reaction.

3.3. Case III. Bönnemann's nanocluster systems: a wide range of metals and extensive use of nanoclusters as heterogeneous catalysts

3.3.1. Synthesis and characterization

Helmut Bönnemann et al. at the Max-Planck-Institut für Kohlenforschung have developed general routes for the multigram syntheses of 10–100 Å transition metal nanoclusters via the reduction of metal salts in THF by tetraalkylammonium hydrotriorganoborates, a route which they have applied to most metals in groups 6–11 [57,137–142], Fig. 13.

---

[8] There is also a need for additional, *quantitative*, ligand poisoning studies of nanocluster catalysts, especially with a range of different ligands designed to poison different types, and geometry, sites. Such studies hold the promise of providing some of the best data yet on the number of types, and their specificities, of different metal sites on nanocluster and nanocolloid catalysts. Such poisoning studies are likely to also be important in providing the next generation of nanocluster-based, *high selectivity*, ideally *single-site* homogeneous and heterogeneous catalysts.
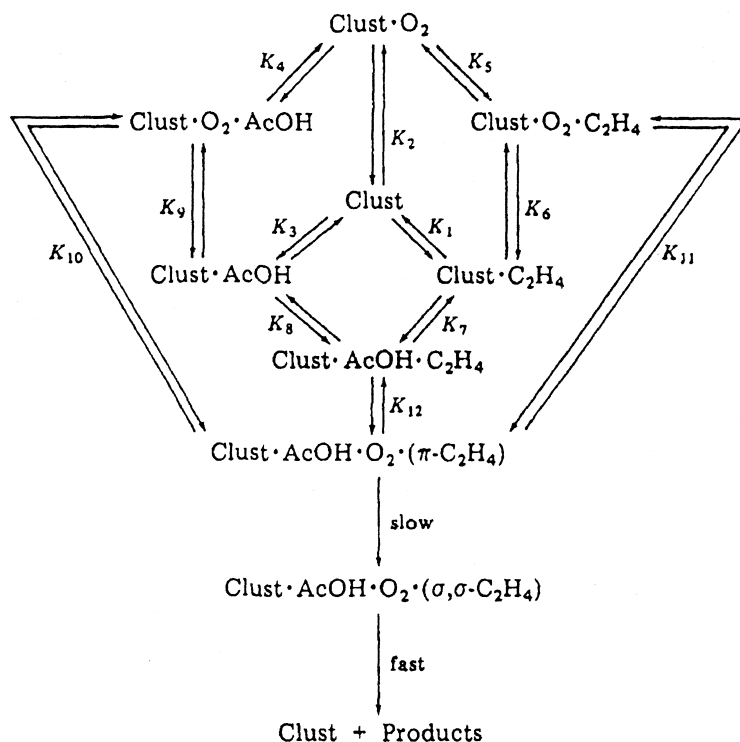
Fig. 12. Proposed mechanism [20] of ethylene oxidation by the $Pd_{\sim 561}phen_{\sim 60}O_{\sim 60}(PF_6)_{\sim 60}$ cluster (abbreviated as 'Clust').

One typical preparative route is shown in Eq. (3), taken from one of Bönnemann's papers [57], where M = metals of groups 6–11; X = Cl, Br; $\nu = 1,2,3$; and R = alkyl, C_6–C_{20}.

$$MX_\nu + \nu NR_4(BEt_3H) \rightarrow M_{colloid} + \nu NR_4X + \nu BEt_3 + \nu/2\,H_2 \uparrow \qquad (3)$$
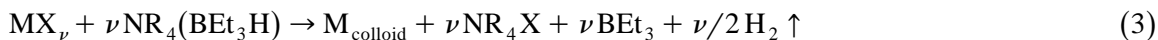
One of the advantages of this preparative route is that the stabilizing agent (the NR_4^+ groups) can be combined with the reducing agent, foregoing the need to add excess stabilizing or reducing agent (as required in their earlier syntheses [139]). Once the THF is removed by evacuation, the metal nano-colloid is redissolved and then precipitated by the addition of either pentane, ether, or ethanol,

Fig. 13. Chart showing the elements Bönnemann et al. have used to prepare nanometal colloids and powders (adapted from Ref. [57]).

allowing collection of the nanoclusters as a powder. The reaction is done at mild temperatures, often 50°C or less, and the filtered colloidal solutions are stable for months (although no supporting TEM evidence for their non-aggregation has been published). Variations on this procedure include the use different reductants (such as H_2, formic acid, LiH, and $KBEt_3H$) [139,141], the use of different metal precursors (such as metal acetates and mixed halides [140,141]) and the addition of different stabilizing agents and surfactants (such as Aliquot 336, $CH_3N[(CH_2)_7CH_3]_3Cl$) to change the solubility properties of the resulting nanoclusters [141]. This synthesis has also been used to synthesize bimetallic metal colloids (such as Pt/Rh) by co-reduction of the metal precursors [57]. Overall, these and the other nanoclusters prepared by these routes are less well characterized *compositionally*.

TEM images of Bönnemann's particles show metal cores that range in average size from 13 Å Ru_n clusters to the 100 Å Au_n clusters. HR-TEM images of the Ir clusters have been published, and metal elemental analyses show metal contents of isolated nanoclusters ranging from 11.3% for iron to 85.1% for platinum. (Boron from the BEt_3H^- reductant is typically found as a 0.5–1.2% impurity in the resultant nanoclusters [140]). Neither XPS or EDS showed halogen or nitrogen present in the nanoclusters under ultra high vacuum conditions, leading the authors to propose that under high-vacuum conditions of the instrument, the stabilizing layer of $R_4N^+X^-$ is removed [139]. X-ray photoelectron spectroscopy and X-ray absorption spectroscopy indicate that the core of $N(CH_3)_2$dodecyl$(CH_2)_3SO_3$-stabilized Rh particles consists of zerovalent metal atoms, but also indicates that some $RhCl_3$ starting material is unreduced and thus remains present [143]. Hence, at least some of these nanoclusters (e.g., Rh) are inhomogeneous.

Despite extensive use of this synthetic procedure, the *mechanism* of metal colloid formation in these systems is not well established. It is claimed that ''the NR_4^+ salts, which are formed in high local concentration at the reduction centre, act as efficient ligands and prevent aggregation of the metal'' [139]. Stabilization presumably occurs as the cationic alkylammonium groups surround the probably *anion-coordinated, and thus negatively-charged metal particle*, with the alkyl groups providing solubility and stability in non-aqueous solvents. More recent X-ray absorption near edge structure (XANES) investigations of Cu nanoclusters suggest that an intermediate Cu^+ state forms prior to nanoparticle nucleation [144].

The data do reveal that the choice of anion is important [140]: for instance, the reduction of $[(C_8H_{14})_4N]_2Pd\mathbf{Cl}_4$ by H_2 gives only metallic precipitate; the reduction of $[(C_8H_{14})_4N]_2Pd\mathbf{Br}_4$ does not occur, even at 50 bar H_2; while the reduction of $[(C_8H_{14})_4N]_2PdCl_2Br_2$ by H_2 yields 40 Å Pd nanoclusters, but only after 336 h [140]. No reason for these differences was provided.

Bönnemann has also reported the synthesis of metal colloids that are putatively only *solvent-stabilized* [141,145]. Reducing $TiCl_4 \cdot 2THF$ with $K[BEt_3H]$ in THF yields very small (< 8 Å), extremely oxophilic, ether soluble clusters formulated as '$[Ti^0 \cdot 0.5THF]_x$'. These are claimed to be stabilized against agglomeration by coordinated ether molecules alone, Fig. 14.

XPS shows that the clusters consist of zero-valence titanium while X-ray absorption near edge structure (XANES), EXAFS, and XPS indicate that there is considerable bonding interaction between the titanium atoms and the THF molecules [145]. Gas-uptake, protonolysis, and $K[BEt_3H]/K[BEt_3D]$ crossover experiments indicate that the metal particles grown from $TiCl_4 \cdot 2THF$ or $TiCl_3 \cdot 3THF$ contain varying amounts of residual hydrogen, and X-ray diffraction and EDX show that a small amount ($< 10\%$) of KCl remains with the clusters [141]. The Cl^- are, however and again, presumably a major source of electrostatic double-layer, Columbic-repulsion type of stabilization of the nanoclusters. The similar reduction of Zr, V, Nb and Mn halides also results in the formation of THF-stabilized colloidal particles [146]. Thioethers have also been used as stabilizing solvents [57].
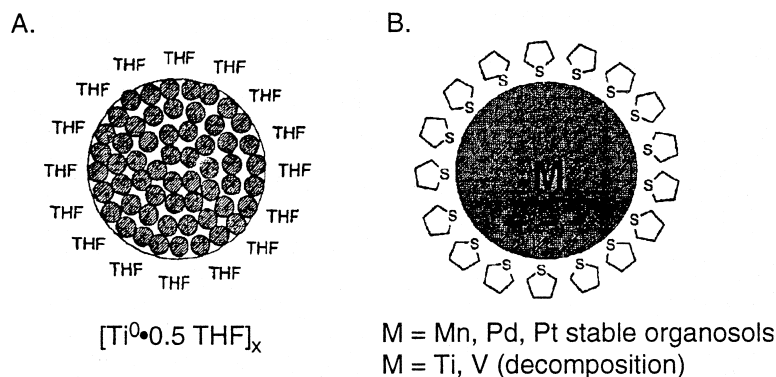
Fig. 14. (A) Representation of Bönnemann's ether-soluble $[Ti^0 \cdot 0.5THF]_x$ clusters taken from Ref. [141]. (B) Representation of Bönnemann's Mn, Pd, and Pt organosols stabilized by tetrahydrothiophene taken from Ref. [57]. Note that these representations *are schematics only*, as some remaining KCl is present (by EDX and mass balance [141]), so that the Cl^- may be coordinating to the Ti and providing anion-based stabilization of the nanoclusters.

3.3.2. Transition-metal nanoclusters as precursors to heterogenous catalysts

Bönnemann et al. report that $R_4N^+X^-$-stabilized nanoclusters precipitate out of solution within 6–7 min after being placed under a H_2 atmosphere [141]; hence, they are ineffective as catalysts *in solution*. However, once immobilized on a solid support, these nanoclusters are active, long-lived heterogeneous catalysts [57].

In what they term the 'precursor concept', Fig. 15, Bönnemann et al. have created heterogeneous catalysts by dipping support materials, such as activated carbon or silicon dioxide Aerosil P 24™, into nanocluster solutions. The clusters adsorb onto the support material with no cluster agglomeration seen by TEM [57]. Worth noting here is that immobilization of transition metal nanoclusters [109,123], as well as other types of metal carbonyl clusters [147], on solid supports have been studied as earlier examples of metal clusters as precursors to heterogeneous catalysts.

The authors report that the activity and lifetime of this type of catalyst is higher than that of the corresponding, commercially available catalysts. For instance, the activity of a 5% colloidal Rh/charcoal (with Rh particles 12–22 Å in diameter) is 244% higher than traditional industrial 5% Rh/charcoal catalysts (with large metal agglomerations and minor fractions of 10–50 Å Rh particles)
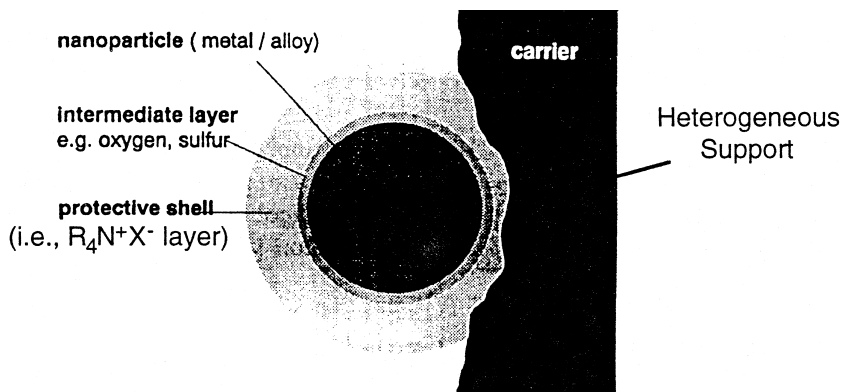

Fig. 15. Idealized, pictorial representation of the heterogeneous catalyst preparation proposed by Bönnemann et al. [57].

for the hydrogenation of butyronitrile [57]. Unfortunately, however, these values are not corrected for the number of exposed atoms in either case. In the case of Bönnemann's supported Pd nanocluster catalysts, these materials exhibit 96,000 turnovers (for an unknown number of exposed Pd atoms) in the hydrogenation of cyclooctene, compared to 38,000 turnovers from an industrial Pd/charcoal catalyst (on a per-exposed-Pd-atom-basis, determined by chemisorption [57]). This enhanced lifetime is attributed to the protective alkylammonium shell, which the authors believe allows small molecules like H_2 and O_2 to pass while preventing direct contact with catalyst surface poisons. Such observations may not be trivial, but instead may point the way to a new generation of ligand-tailored catalysts [14] with improved lifetimes or selectivities (or both). Bönnemann also shows that the activity of these catalysts can be increased by (i) adding small (albeit not exactly known) amounts of oxygen, (ii) doping the Rh catalyst with 0.2% titanium, (iii) pretreatment with acid, or (iv) decreasing the length of the alkyl chain in the stabilizing group [57]. Nanoclusters offer the possibility to understand these effects at close to the molecular level, but such more-detailed studies have yet to appear.

The $[Ti^0 \cdot 0.5THF]_x$ clusters, once deposited on a support, are also active in the hydrogenation of Ti and Zr sponges and nickel hydride battery alloy [146]. Interestingly, however, the hydrogenation of Ti sponge by $[Ti^0 \cdot 0.5THF]_x$ clusters at 60°C and 150 bar H_2 proceeds *only after a 5 h induction period* (a period which varies, depending upon H_2 pressure and temperature) [146], an observation that remains unexplained. The observation of the induction period demands that the catalyst is *not* the $[Ti^0 \cdot 0.5THF]_x$ clusters, for the general reasons developed elsewhere [52].

More recently Bönnemann has performed enantioselective hydrogenation of ethylpyruvate to (*R*)-ethyl lactate using chiral-ligand-stabilized Pt colloids suspended in an acetic acid/methanol solution, Eq. (4) [16]. These studies mirror, of course, the extensive studies of this same reaction using traditional heterogeneous Pd and other catalysts (see the references summarized elsewhere [16]).

Dihydrocinchonidonium

(4)
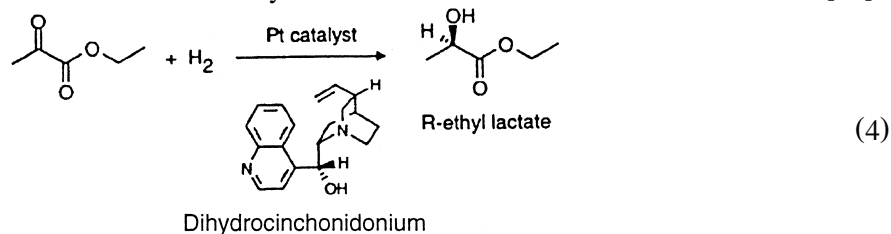
The catalytic reaction results in an unexceptional enantiomeric excess of 76%; the activity of the colloids decreases with increasing particle size (ranging in size from 12 Å to ~ 38 Å). Furthermore, decreasing the concentration of the chiral stabilizing ligand causes a decrease in catalytic activity without affecting the enantiomeric excess [16]. The key issue here appears to be that of how to get nanocluster (or heterogeneous) catalysis % ee values above the more common 75–85%, and into the more useful, ≥ 98% level.

Bönnemann et al. have also reported that bismuth-promoted bimetallic Pd–Pt/C catalysts (made from $N(Octyl)_4Cl$-stabilized bimetallic Pd–Pt nanoclusters) oxidize glucose to gluconic acid with superior activity and selectivity relative to industrial heterogeneous Pd–Pt catalysts [148]. Exact controls comparing the best previous industrial catalysts to the nanocluster catalyst, and under identical reaction conditions, were not reported, however.

The main advantages of Bönnemann's systems include the large scale preparation (several grams) and the wide range of metal nanoclusters available. Disadvantages include the use of metal salts as precursors (some of which are hard to obtain in pure form, e.g. 'IrCl$_3$'), some synthetic irreproducibil-

ity (some of which may be related to the use of metal salt precursors, as in the case of IrCl$_3$; see footnote 19 elsewhere [1]), and a lack of exact compositional characterization of the resultant wide range of nanocluster materials.

3.4. Case IV. Reetz's $NR_4^+X^-$-stabilized nanocluster systems

3.4.1. Electrochemical synthesis

Manfred Reetz et al. at the Max-Planck-Institut für Kohlenforschung have developed an impressive, large-scale, size-selective *electrochemical-based* synthetic procedure for the preparation of transition metal nanoclusters [149]. Using an electrochemical cell in which a sacrificial anode is used as a metal source and a supporting electrolyte doubles as a nanocluster stabilizing agent, Reetz reported in 1994 the synthesis of 14 Å, 31 Å, and 48 Å $(C_8H_{17})_4N^+Br^-$-stabilized Pd nanocluster distributions in CH$_3$CN/THF [150]. Significant aspects of this technique are that (i) nanocluster size can be controlled by varying the current density (higher current densities give smaller particles; see the equation given elsewhere [72]); (ii) isolation of the clusters is simple—they precipitate out of solution as black powders when formed; and (iii) the R$_4$N$^+$X$^-$-stabilized clusters are redissolvable in nonaqueous solvents at concentrations up to 1 M [151]. Furthermore, (iv) the reaction proceeds with high yields ($>95\%$) and can be performed on a moderate scale (hundreds of milligrams). This synthetic method can be applied to other, easily oxidized metals such as Ni, Cu, and Au (although the sacrificial nature of the electrode leads to one of limitations of the electrochemical synthesis method). And, by changing the supporting electrolyte/stabilizing agent, the solubility of the resulting nanoclusters can be varied from nonpolar solvents like pentane (using tetraoctadecylammonium bromide) to water (using sulfobetaine 3-(dimethyldocecylammonio)propanesulfonate · LiCl) [149,150]. More recently, this procedure has been used to grow nanoclusters from metals that are not easily oxidized (such as Pt, Rh, Ru and Mo) by using the corresponding metal salt in place of the sacrificial anode [152]. Note, as Fig. 16 below shows, the metal salt diffuses to, and is reduced at, the cathode. Bimetallic Ni/Pd, Fe/Co and Fe/Ni nanoclusters have also been grown [153].

One drawback to this method is that nanocluster formation and growth cannot be followed *directly*, limiting the amount of mechanistic information that can be collected. (Reetz himself states that the ''precise mechanism of colloid formation is difficult to determine'' [149]). However, a rudimentary mechanism has been proposed [149], Fig. 16, consisting of (i) dissolution of the sacrificial anode (i.e., in this case by oxidation of Pd^0 to Pd^{2+}), (ii) metal ion migration to the cathode, (iii) reductive metal adatom formation at the cathode interface, (iv) aggregation of the metal adatoms, (v) stabilization by 'self organization' of the ammonium ions around the metal core, and finally (vi) precipitation. There is, however, no kinetic or other direct evidence for the proposed mechanism.

Reetz reports the electrochemical synthesis of 80–100 Å Pd nanoclusters in propylene carbonate in which no R$_4$N$^+$X$^-$ stabilizing agent is used [23]. NaCl is, however, used as an electrolyte and 5% ethanol is also present; hence, the resultant nanoclusters are most likely Cl$^-$ stabilized nanoclusters, an important point not addressed in this work. As the reaction proceeds, the solution turns black as the Pd nanoclusters are formed, but no bulk metal formation is observed. A 0.2 M propylene carbonate solution of Pd nanoclusters is stable at 140–155°C for several days ''without showing any sign of Pd powder formation'' [23]. This is an important observation, one that suggests the use of polar solvents for higher-stability nanoclusters. No TEM evidence was provided on whether or not the Pd nanoclusters aggregate at these higher temperatures, however. And, unfortunately, once the solution is evacuated to dryness, bulk metal is formed *which cannot be redispersed in solution* [23], limiting the use and storage of these presumably Na$^+$Cl$^-$ stabilized Pd nanoclusters to their original solutions
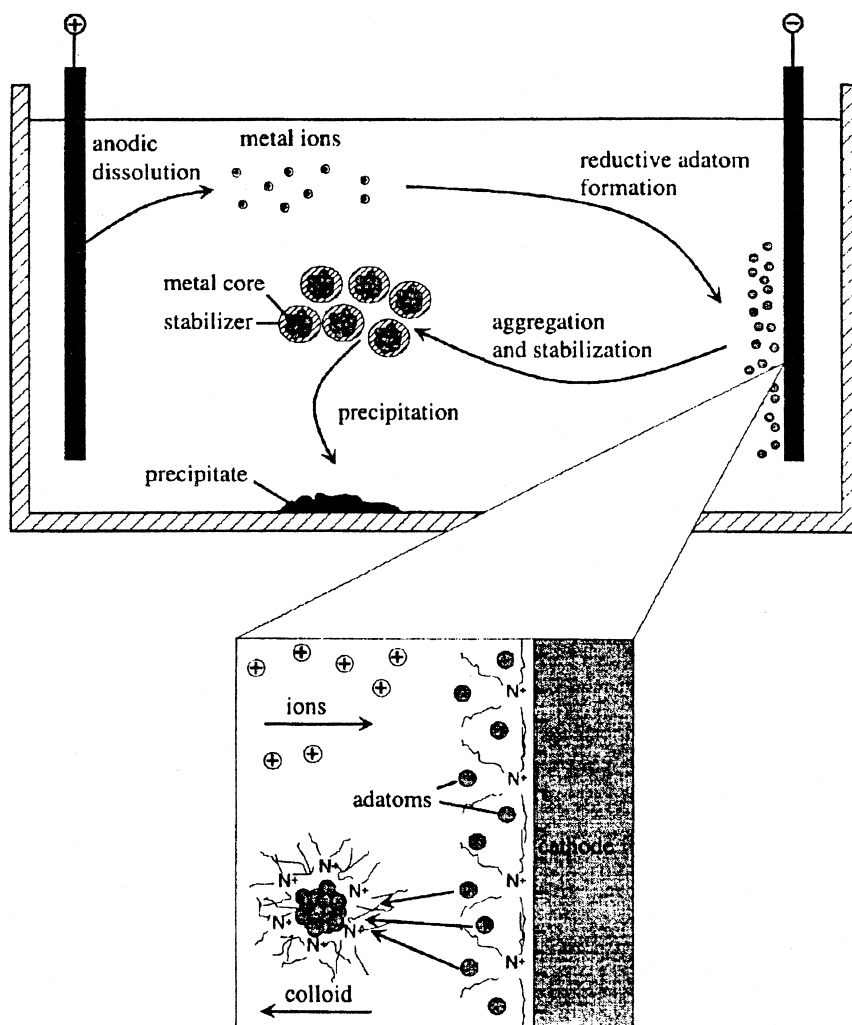
Fig. 16. Reetz et al.'s postulated mechanism [149] for the formation of his electrochemical synthesized $R_4N^+X^-$-stabilized nanoclusters.

only. [An alternative preparation of solvent-stabilized nanoclusters involves thermal decomposition of $Pd(O_2CMe)_2$ in propylene carbonate at 100°C for 3 h; sonication speeds up the reaction in this case [23]. The Pd clusters grown and isolated (as a dry powder) by this route also *cannot* be redissolved]. These are important findings, given that the $(C_8H_{17})_4N^+Br^-$-stabilized Pd nanoclusters grown in CH_3CN/THF are isolable and redissolvable, whereas the Pd clusters grown in propylene carbonate/NaCl/ethanol are not. The implication is that greater stability is provided by longer-chain R_4N^+ cations. However, the exact role of the different cations, anions, and solvent in allowing isolable, resuspendable, and catalytically active transition metal nanoclusters remains to be worked out.

3.4.2. Characterization

Reetz et al. were the first to report a combined TEM/STM study of Pd nanoclusters stabilized by a series of alkylammonium bromides ranging from $(C_4H_9)_4N^+Br^-$ to $(C_{18}H_{37})_4N^+Br^-$ [99]. Using TEM to determine the diameter of the Pd metal core (d_{TEM}), and STM to determine the total diameter

of the nanocluster (d_{STM}), Fig. 17, he calculates a mean diameter difference ($2\Delta = d_{STM} - d_{TEM}$). Reetz et al. find that in all cases, the d_{STM} is larger than the d_{TEM} and that the difference in diameters is accounted for by (only) the length of the alkyl chain in the stabilizing agent. Furthermore, he calculates theoretical values of the stabilizing layer thickness, Δ, using MM2 force field calculations and finds that the theoretical values are in 'excellent' [99] agreement with the experimentally-determined values.

This work is an important, early effort in the characterization of ligand-stabilized nanoclusters; however, there still exists some uncertainty surrounding these results. To begin, the authors themselves cannot explain the mechanism by which the electrons tunnel from the STM tip through the $R_4N^+Br^-$ groups [99]. Furthermore, they assign the larger STM diameters vs. TEM diameters to the alkylammonium groups alone, neglecting the Br^- anions that are almost surely on the present of the nanocluster's surface, a point first made elsewhere [1]. Moreover, it has recently been discussed how tip and surface effects can lead to overestimated particle diameters when individual particles are imaged [100,102].

Another technique that Reetz et al. have used to characterize Pd/Pt bimetallic clusters, and their oxidized/oxide analogs, is extended X-ray adsorption fine structure (EXAFS). EXAFS suggests that the amount of metal oxide present in the outer shell is larger than in the core [154] (which, however, is in direct disagreement with an earlier statement that little, if any, oxidized Pd is present in the nanoclusters [150]). These data argue that, as one might expect, many nanoclusters will be air-sensitive and, therefore, have some oxide on their surface or in their bulk if they are not rigorously protected from air. The air sensitivity of transition metal nanoclusters is a point which requires further experimental scrutiny for many of the transition metal nanoclusters described in the literature. EXAFS also shows a small amount of the metal bromide contaminate (or stabilizer; is not entirely clear which) is present, in agreement with elemental analysis data [150].

Reetz et al. have also shown that cyclic voltammograms of 14 Å Pd nanoclusters show that peak potential shifts agree with theoretical values for metallic Pd particles of that size [149]. The size-dependent redox [155] and ionization potentials (IP) [156] of Ag_n nanoclusters are available from other work [155,156], studies which show, for example, a lower IP with increasing cluster size, n [156].
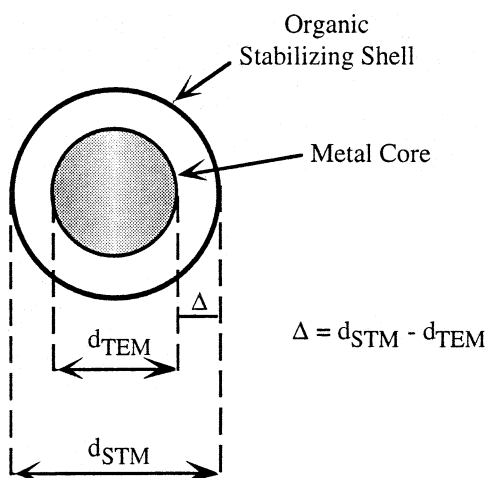

Fig. 17. Distances Measured by TEM and STM Microscopies (adapted from Reetz et al.) [99]. Note, however, the ambiguity about where the (omitted) inorganic anions (Cl^-, or other X^-) fit into this picture.

3.4.3. Catalytic properties of Reetz's nanoclusters

Reetz et al. have examined the catalytic activity of Pd nanoclusters both as colloidal solutions (for the Heck and Suzuki carbon–carbon bond forming reactions [23]) and immobilized on an Al_2O_3 support as traditional heterogeneous catalysts (for olefin hydrogenation [157] or Heck reactions). In one of the first studies to use soluble nanoclusters to catalyze the formation of carbon–carbon bonds, Reetz et al. showed that propylene-carbonate stabilized Pd nanocluster solutions catalyze the Heck reaction between styrene and chlorobenzene to form the corresponding carbon–carbon coupling product at about 30% yields; when bromobenzenes are used, the yields increase to between 79 and 97%, with 19–100% conversion [23]. Likewise, Reetz's original $(C_8H_{17})_4N^+Br^-$-stabilized Pd clusters and $(C_4H_9)_4N^+Br^-$-stabilized Pd/Ni bimetallic clusters are effective as carbon–carbon bond forming Heck and Suzuki reaction catalysts, with the Pd/Ni bimetallic clusters being the most efficient [22]. (It is not known whether this is due to catalysis by both metals or possible effects that nickel might have on the cluster's morphology). Reetz has also demonstrated that Ti clusters induce McMurry-type coupling of aldehydes and ketones [21], and that Ni clusters catalyze the $[3 + 2]$ cycloaddition of methylenecyclopropane to methyl acrylate [24]. The highest reported yield of cycloaddition product is 35%, obtained after 24 h at 130°C, representing 39 total turnovers [24].

Reetz et al. have also developed a class of heterogeneous catalysts by impregnating Al_2O_3 pellets with immobilized Pd, Ni, or Pt/Sn nanoclusters [157]. One useful feature of this preparative route is that, by taking into account pore diameter and nanocluster size, one can design catalysts in which the metal particles of a specified size are found solely on the outer surface of the support, without deep penetration into the support material. The stated goal of this approach is to minimize any potential diffusion problems into the core of the support that might occur during catalysis. Reetz calls these 'cortex' (i.e., the outer part or external layer) catalysts [157]. Immobilization occurs without agglomeration or any change in the metal core size as demonstrated by TEM. Washing removes up to about 95% of the $R_4N^+X^-$ stabilizer in some cases, leaving well-defined, unagglomerated, crystalline clusters of known size immobilized on the surface of the support. This is an active type of catalyst as well: when a Pd nanocluster 'cortex' catalyst (5% Pd on Al_2O_3) is used in the hydrogenation of cyclooctene, its activity is more than 3 times that of a comparable, commercially-available industrial 5% Pd on Al_2O_3 catalyst [157]. Unfortunately, however (i) no correction for the number of exposed Pd atoms in the two catalysts was reported, and (ii) no evidence that diffusion plays a part in these rate differences was presented (i.e., and under the reaction conditions). Hence, the concept of 'cortex' catalysts remains to be definitively tested.

Interestingly, the reactivity of the nanoclusters changes once they have been deposited: whereas *solutions* of propylene carbonate stabilized Pd nanoclusters were active Heck reaction catalysts, once the Pd nanoclusters are immmobilized on Al_2O_3, they are active only at the 1% level after 17 h for the Heck reaction [23]. No explanation for this finding was given. A needed, but unreported, key control experiment here is whether or not the supported Pd catalyst has retained its activity for other reactions. If so (i.e., if the supported catalyst has not just been totally inactivated), then this is an important observation; understanding it could lead to insights in how to design *high selectivity* catalysts.

3.4.4. Other properties of Reetz's nanoclusters

Reetz has also studied the magnetic properties of $(C_8H_{17})_4N^+Br^-$-stabilized Co clusters [158], finding that superparamagnetic Co clusters turn from blackish-brown to olive-green within a few hours as they are slowly oxidized by dry oxygen [159]. Oxygen-uptake experiments show that a stoichiometric amount of cobalt(II) is formed as oxidation occurs. Oxidation of the cobalt clusters

causes the magnetic susceptibility to fall away completely as the clusters become diamagnetic. The lattice constant, obtained from the electron diffraction rings, is in good agreement with that of bulk CoO, the only cobalt oxide that is fcc [159]. Note also that if the CoO clusters come in contact with moisture from the air, then the TEM images show that the particles agglomerate into larger particles that are between 1000 Å and several mm in size [159]. Obviously, water is a key ingredient in the stability of such CoO, and perhaps other metal oxide, clusters.

Reetz et al. have also developed a lithographic process capable of forming lines of Pd metal as small as 50 nm in width, accomplished by spin-coating a THF solution of 20 Å $(C_8H_{17})_4N^+Br^-$-stabilized Pd clusters onto a GaAs substrate followed by electron-beam etching [12,160]. In addition, Reetz et al. have shown that 59 Å $(C_8H_{17})_4N^+Br^-$-stabilized Pd clusters self-assemble into hexagonal-close-packed three-dimensional super lattices on carbon grids [161], an observation that could be important implications for nanoscale engineering or the construction of single-electron tunneling devices.

3.5. Case V. Polyoxoanion- and tetrabutylammonium-stabilized transition-metal nanoclusters

3.5.1. Synthesis and characterization

The Finke research group entered nanocluster chemistry as a result of in-depth kinetic and mechanistic studies [162] of the identity of the active catalyst which results when the polyoxoanion-supported Ir(I) organometallic complex $[(n\text{-}C_4H_9)_4N]_5Na_3[(1,5\text{-}COD)Ir \cdot P_2W_{15}Nb_3O_{62}]$, [9] Fig. 18, is placed under H_2, with or without cyclohexene as a substrate for hydrogenation catalysis.

Eq. (5) shows the overall, average stoichiometry of the formation of the resultant $Ir(0)_{\sim 300}$ nanoclusters. Through detailed kinetic, mechanistic, and catalyst characterization studies, they report that the reduction of this discrete complex under hydrogen, in acetone, and with 1.65 M cyclohexene present results in the formation of a new subclass of nanoclusters, *polyoxoanion- and tetrabutylammonium-stabilized*, near-monodisperse (i.e. $\pm 15\%$ size dispersion [1]) 20 ± 3 Å $Ir(0)_{\sim 300}$ nanoclusters [15]. The same reaction performed in the absence of cyclohexene leads to larger, 30 ± 4 Å $Ir(0)_{\sim 900}$ nanoclusters. Note that these nanocluster *distributions* center about the two magic numbers, namely the full shell cluster geometries M_{309} and M_{923}.

$$300 \, [(1,5\text{-}COD)Ir \cdot P_2W_{15}Nb_3O_{62}]^{8-} \, + \, 750 \, H_2 \longrightarrow$$

$$300 \, \bigcirc \, + \, 1 \, Ir(0)_{\sim 300} \, + \, 300 \, P_2W_{15}Nb_3O_{62}^{\,9-} \, + \, 300 \, H^+ \tag{5}$$
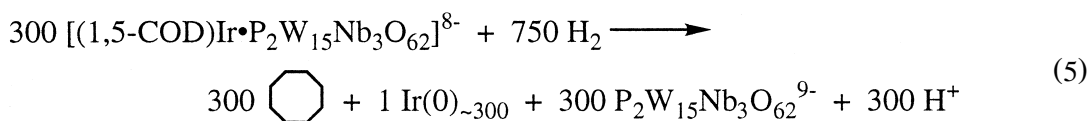
Fig. 19 shows an idealized, pictorial representation of the resulting nanoclusters, with the 20 Å $Ir(0)_{\sim 300}$ and the 12×15 Å $P_2W_{15}Nb_3O_{62}^{9-}$ polyoxoanion scaled to their approximate relative sizes [1].

The Ir(0) nanoclusters vie as the best compositionally characterized nanoclusters in the literature [1], having been characterized by TEM, HR-TEM, STM, electron diffraction, elemental analysis, ultracentrifugation solution molecular weight, FAB-MS, electrophoresis, ion-exchange chromatography, IR spectroscopy, and H_2 uptake stoichiometry [15]. Their formation stoichiometry is crucial; it

---

[9] For $(1,5\text{-}COD)M \cdot P_2W_{15}Nb_3O_{62}^{8-}$ synthesis and characterization: see Refs. [170–173].
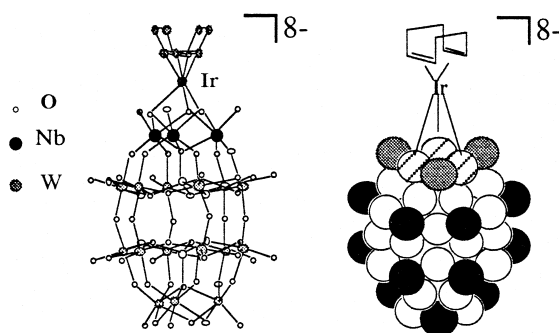
Fig. 18. Ball and stick (leftmost) and space-filling (rightmost) representations of $[(n\text{-}C_4H_9)_4N]_5Na_3[(1,5\text{-}COD)Ir \cdot P_2W_{15}Nb_3O_{62}]$. In the space-filling representation the black circles represent terminal M = O oxygens, whereas the open, white circles represent M–O–M bridging oxygens. The five $[(n\text{-}C_4H_9)_4N]^+$ and three Na^+ counter-cations are omitted for clarity.

proves that the Ir(0) core is *uncharged*, a point rarely examined much less demonstrated in the nanocluster literature. Electron diffraction shows that the metal core of the nanoclusters is composed of ccp Ir(0) metal. Elemental analysis and solution molecular weight give an average molecular formula of $[Ir(0)_{\sim 300}(P_4W_{30}Nb_6O_{123}^{16-})_{\sim 33}](Bu_4N)_{\sim 300}Na_{\sim 228}$. FAB-MS, and IR spectroscopy con-
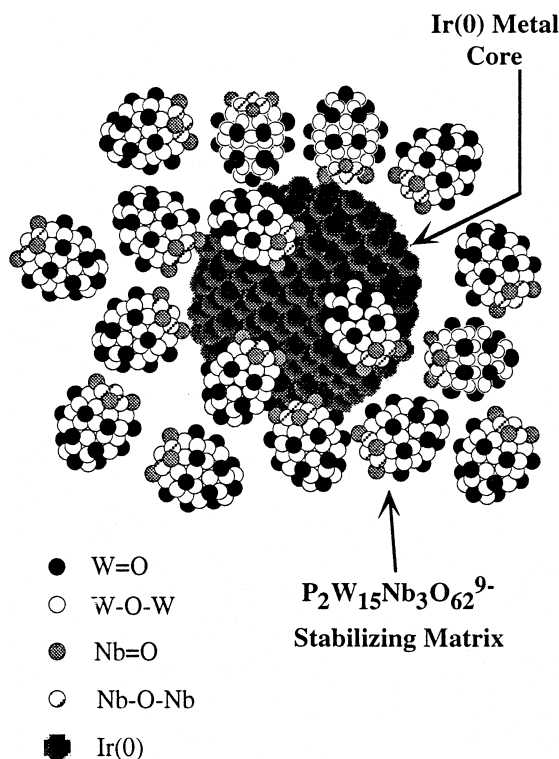
Fig. 19. Idealized, roughly-to-scale representation of a $P_2W_{15}Nb_3O_{62}^{9-}$ polyoxoanion and Bu_4N^+ stabilized 20 ± 3 Å $Ir(0)_{\sim 300}$ nanocluster, $[Ir(0)_{\sim 300}(P_4W_{30}Nb_6O_{123}^{16-})_{\sim 33}](Bu_4N)_{\sim 300}Na_{\sim 228}$. For the sake of clarity, only 17 of the polyoxoanions are shown, and the polyoxoanion is shown in its monomeric, $P_2W_{15}Nb_3O_{62}^{9-}$ form (and not as its Nb–O–Nb bridged, anhydride, $P_4W_{30}Nb_6O_{123}^{16-}$ form). The ~ 330 Bu_4N^+ and ~ 228 Na^+ cations have also been omitted, again for the sake of clarity.

firm the presence of the polyoxoanion stabilizing agent. Significantly, electrophoresis and ion-exchange chromatography show that in solution, the clusters *contain an overall negative charge*, despite the overall neutral Ir(0) core. This observation indicates that the negatively-charged stabilizing polyoxoanion—the only anion present—must be binding to, and thus is crucial in stabilizing, the Ir(0) nanoclusters in solution.

It remains to be proven exactly how special the $P_2W_{15}Nb_3O_{62}^{9-}$ polyoxoanion is, or is not, in comparison to other anions or polyanions, and such studies are in progress [174]. So far the $P_2W_{15}Nb_3O_{62}^{9-}$ polyoxoanion is the best at providing both high stabilization and also high catalytic activity vs. other X^- or polyanions ($X^- =$ halides, $P_3O_9^{3-}$, $SiW_9Nb_3O_{40}^{7-}$ [162]); additional studies of other especially polyoxo- and other poly-anions are in progress [174]. The key concept is already reasonably clear, however: it is the ''*combined high charge* plus *significant steric bulk present intrinsically* within the *poly*anion and *poly*-Bu_4N^+ cation components of $(Bu_4N^+)_9(P_2W_{15}Nb_3O_{62}^{9-})$'' [15]. A pictorial view of this combined, intrinsically high charge and steric bulk stabilization is provided in Fig. 20.

Also of note here is the value of catalytic screening; it was an up-front survey during 1982–1987 of $[(1,5\text{-COD})M^1(CH_3CN)_2]^+$ (M = Ir, Rh) with a variety of polyoxoanions for their hydrogenation catalysis that led to the present polyoxoanion-stabilized nanoclusters [175]. It was from those survey studies that $P_2W_{15}Nb_3O_{62}^{9-}$ emerged as the polyoxoanion of choice, and at least vs. the polyoxoanions available and screened at that time ($SiW_9V_3O_{40}^{7-}$, $SiW_9Nb_3O_{40}^{7-}$, $P_2W_{18}O_{62}^{6-}$, $P_2W_{15}V_3O_{62}^{9-}$, $P_2W_{15}Nb_3O_{62}^{9-}$) [175].

The use of this polyoxoanion as a nanoparticle stabilizing agent is without precedent in the literature, and gives rise to most of the unique aspects of these nanoclusters. Another unique aspect is that these clusters are synthesized from a well-defined and well-characterized molecular precursor, under complete air- and water-free conditions, using H_2 as a reductant (as compared to using
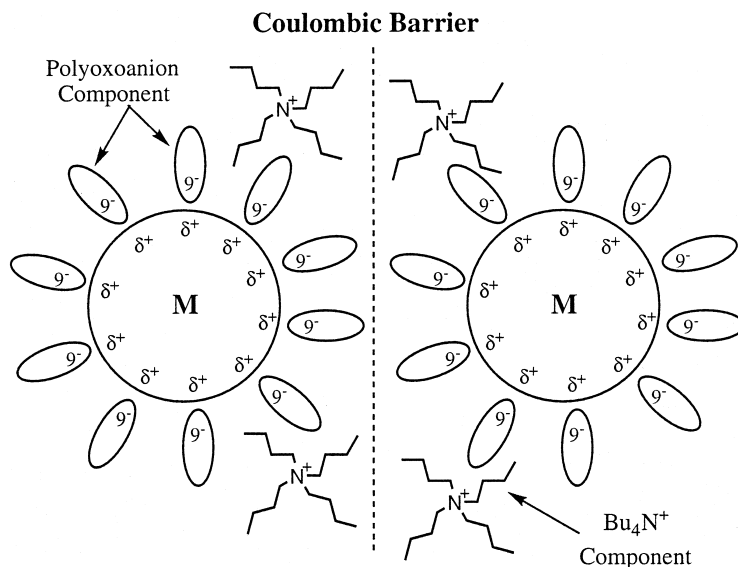
Coulombic Barrier

Fig. 20. Depictation of the barrier created by the combined, high charge ('inorganic'; $P_2W_{15}Nb_3O_{62}^{9-}$) electrostatic and steric ('organic'; Bu_4N^+) colloid-type stabilization of transition metal nanoclusters provided by the polyoxoanion component and its associated Bu_4N^+ cations.

$R_4N[BEt_3H]$, for example [141]), so that no oxides, hydroxides, water, halides, or boron contaminate the metal surface of the nanoclusters. The Ir(0) nanoclusters are, therefore, a system with an extremely clean, exposed, and (catalytic data show [162]) chemically reactive surface.

3.5.2. Mechanistic studies of nanocluster formation and growth

A distinct advantage of this nanocluster system is that nanoparticle formation and growth can be followed in real time, albeit somewhat indirectly. This, in turn, allows the collection of the first kinetic and mechanistic information on the formation and growth of modern, well-characterized transition-metal nanoclusters, some of the first more quantitative and detailed information on soluble particle growth since the classic studies of LaMer in the 1950s on the formation of sulfur sols [52].

Two methods can be used to follow nanocluster formation and growth [176]: either following hydrogen pressure vs. time during a cyclohexene hydrogenation experiment, or, more directly, following the loss of the precursor by the 1:1 conversion of its cyclooctadiene ligand to cyclooctane by GLC. The hydrogen pressure vs. time curve for the formation of Ir nanoclusters is sigmoidal in shape and shows a characteristic, reproducible induction period. Fig. 21 shows that this curve can be *quantitatively* fit to the analytic equation derived for the first two, rate-determining steps of the surprisingly simple, three-step mechanism for nanocluster formation shown in Scheme 1—a reaction that must of necessity (by the stoichiometry back in Eq. (5)) have $\gg 300$ steps [52].

Curve fitting either the H_2 uptake (or, equivalently, the cyclohexene loss) or the GLC-determined conversion of cyclooctene in the precursor to cyclooctane yields the same values for k_1 and k_2 within experimental error for the $Ir(0)_{\sim 300}$ example [52].
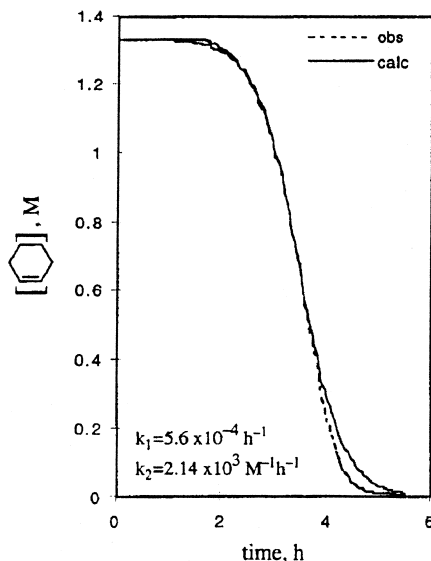
Fig. 21. A typical curve-fit, taken from Ref. [52], of the loss of cyclohexene (determined by following the loss of hydrogen pressure vs. time) demonstrating the excellent curve fit to the nucleation plus autocatalysis, then hydrogenation, three step kinetic model. The resultant rate constant k_2 has been corrected by the mathematically required 'scaling' and 'stoichiometric' factors [52], correction factors required to take into account, respectively, the changing size of the nanocluster's surface and the use of the hydrogenation of 1400 equivalents of cyclohexene to monitor the nanocluster formation reaction. (The deviations between the observed and calculated curves late in the reaction are expected, as explained elsewhere [52]).

$$x \left[A \xrightarrow{k_1} B \right] \qquad\qquad \textit{Nucleation} \qquad 1.$$

$$1-x \left[A + B \xrightarrow{k_2} 2B \right] \qquad\qquad \textit{Autocatalysis} \qquad 2.$$

$$\sim1400 \left[B + \text{⬡} + H_2 \xrightarrow[\textit{Fast}]{k_3} B + \text{⬡} \right] \qquad \textit{Fast hydrogenation} \qquad 3.$$

$$\text{Sum:} \quad A + \sim1400\,\text{⬡} + \sim1400\,H_2 \xrightarrow{k_{obs}} B + \sim1400\,\text{⬡} \qquad 4.$$
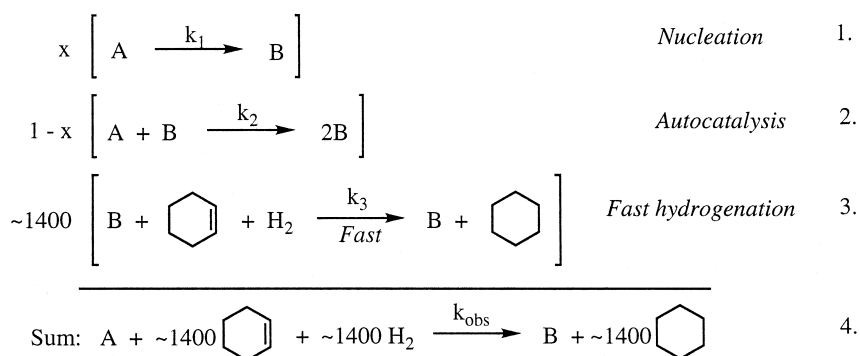
Scheme 1. General three-step mechanistic scheme containing nucleation (induction period), k_1, autocatalysis (nanocluster growth), k_2, and fast olefin hydrogenation, k_3, where A is the precatalyst, $(1,5\text{-COD})\text{Ir} \cdot P_2W_{15}Nb_3O_{62}^{8-}$, and B is the catalyst, the $\text{Ir}(0)_n$ nanoclusters. The sum reaction is a novel use of the 'pseudoelementary step' concept, a method useful for following the kinetics of more complicated, multistep reactions [177–179].

This three step mechanism is composed of a nucleation step (Step 1), an autocatalysis step (Step 2) and a hydrogenation step (Step 3). Since hydrogenation (Step 3) is faster than all other steps in the mechanism, the kinetics of the summation step (4) will be those of steps 1 and 2 (and hence will yield values of the rate constants k_1 and k_2). Furthermore, since measurable hydrogen consumption is due only to step 3 (due to the 1400-fold higher concentration of olefin relative to precatalyst), cyclohexene hydrogenation acts as a valuable 'kinetic reporter reaction' in this system [52]. There is no obvious reason that other nanocluster formation reactions cannot also be followed using this method.

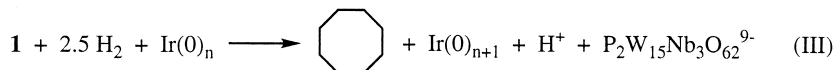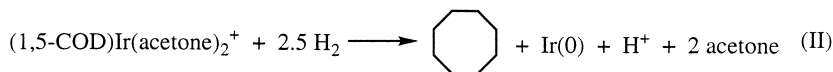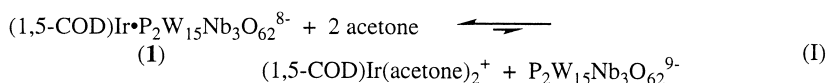The proposed, overall minimum mechanism of nanocluster formation and growth is shown in Scheme 2. While the steps of (i) nucleation, (ii) growth, and then (iii) agglomeration are the expected sequence for any particle growth, the mechanism in Scheme 1 stands as a new mechanism in that its (1) slow, *continuous* nucleation, and (2) *autocatalytic surface growth* were previously unappreciated [10] [180–183]. Moreover, evidence presented elsewhere strongly suggests that this mechanism is operating in most nanocluster systems synthesized by the reduction of metal salts *under hydrogen* [52].

This proposed mechanism holds predictive powers, as any good mechanism should. Born from this proposed mechanism are the following predictions, each of which have been shown to hold true [184]: (i) the nanoclusters will act as 'living-metal polymers', a concept that can be used to grow larger, designed-sized nanoclusters simply by adding the proper amount of metal precursor [184]; (ii) the ratio of growth to nucleation, $R' = k_2/k_1$, should be a predictor of nanocluster size [184]; (iii) the key step in this mechanism, autocatalysis, should provide favorable conditions for the formation of near-monodisperse clusters by separating nucleation and growth in time [52]; and (iv) the autocatalytic surface growth should—and does [184]—predict that more stable, and thus slower growing, full-shell

---

[10] Following our 1997 mechanistic paper [52] in which all prior mechanistic studies of metal or other particle formation that we could find are referenced (see the extensive list of references therein [52]), we recently came across some papers in the pulse radiolysis literature where Ag aggregate formation, analogous to the photographic development process, is studied [180–183]. The words 'autocatalysis' are mentioned in these papers, but convincing kinetic data for autocatalysis is lacking (some of the curves look, instead, bi- to tri-phasic, a point the authors also made [181]). In addition, the pulse radiolytic reduction of Ag^+ by *pulse* radiolysis generated reductant, $\text{Red}^{\cdot-}$, is not closely related to the direct reduction of transition-metal salts by a continuously present reagent such as H_2. However, a closer study of the Ag^+ and the better studied [52] $\text{Ir}(I)^+$ system shows that the net stoichiometries of the two are actually rather similar: $\text{Ag}(0)_n + 2\,Ag^+ + 2\,\text{Red}^{\cdot-} \to \text{Ag}(0)_{n+2} + 2\,\text{Red(oxidized)}$, and $\text{Ir}(0)_n + 2\text{Ir}(I)^+ + H_2 \to \text{Ir}(0)_{n+2} + 2H^+$. (The main difference is probably that Ag^+ is on the surface before the reaction with $\text{Red}^{\cdot-}$, while H_2 is activated on the surface of $\text{Ir}(0)_n$, *before* $\text{Ir}(I)^+$ adds and is reduced.) Hence, the autocatalytic surface growth mechanism may be even more general than argued before [52].

$$(1,5\text{-COD})Ir \cdot P_2W_{15}Nb_3O_{62}{}^{8-} + 2 \text{ acetone} \rightleftharpoons$$

(1)

$$(1,5\text{-COD})Ir(\text{acetone})_2{}^+ + P_2W_{15}Nb_3O_{62}{}^{9-} \qquad \text{(I)}$$

$$(1,5\text{-COD})Ir(\text{acetone})_2{}^+ + 2.5\, H_2 \longrightarrow \bigcirc + Ir(0) + H^+ + 2 \text{ acetone} \quad \text{(II)}$$

$$\mathbf{1} + 2.5\, H_2 + Ir(0)_n \longrightarrow \bigcirc + Ir(0)_{n+1} + H^+ + P_2W_{15}Nb_3O_{62}{}^{9-} \quad \text{(III)}$$

$$n\, Ir(0) \longrightarrow Ir(0)_n \qquad \text{(IV)}$$

Scheme 2. Proposed, more intimate (but still Occam's razor, i.e., minimum) mechanism for the formation of polyoxoanion-stabilized Ir(0) nanoclusters [52].

('magic number') clusters will be formed. The mechanism (v) also predicts that a sequential series of nanoclusters centering about the full-shell, 'magic numbers' can be grown, another prediction that has been verified [184], and (vi) provides the mechanistic insights needed to better design the synthesis of bi- and higher multimetallic nanoclusters, Fig. 22.

Very recently Ahmadi et al. have provided evidence that their shape-selected Pt nanoclusters [51] also grow, as predicted [52], by a surface-growth mechanism [50]. Peng et al. have also recently investigated the kinetics of diffusion limited growth of CdSe and InAs particles [185]. Hence, the previous major holes in our understanding of the mechanisms of nanoparticle growth are beginning to be filled.

3.5.3. Catalysis: Development of 'soluble heterogeneous catalysts'

The polyoxoanion-stabilized nanoclusters, such as $Ir(0)_{\sim 300}$, are important catalyst materials in several ways. First, the polyoxoanion stabilizing anion and its associated R_4N^+—providing both

A (core)   B (core)   C (core)

B | C   A | C   A | B

A/B/C   A/C/B   B/A/C   B/C/A   C/A/B   C/B/A
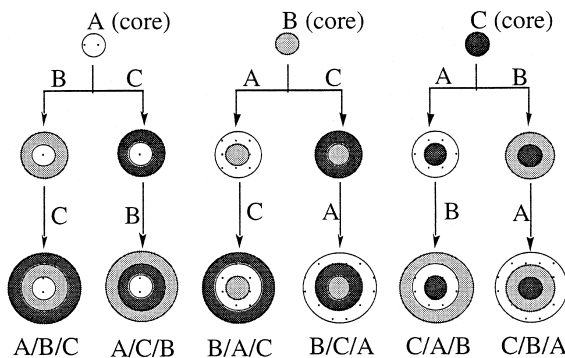
Fig. 22. Illustration of the living-metal polymer approach to the synthesis of multimetallic nanoclusters of, at least in principle, well-defined initial structure and layer thickness. It needs to be emphasized that this scheme *is idealized* and intended only to illustrate the concept involved. It is already known for example, that some bimetallic nanoclusters do *not* show such idealized second layers as illustrated above [115] [See also Ref. 35 elsewhere [184]. In addition, if a lattice or symmetry mismatch exists between the layers, thereby creating a high interfacial energy, it is more likely that imperfect (e.g., mound or island) growth will occur [e.g., as seen in molecular-beam epitaxial growth (Ref. 35c elsewhere [184])]. Layer (atomic) migrations can also occur [115]. However, it is also likely that closer to idealized bi- and higher multimetallic nanoclusters can be obtained by application of the autocatalytic surface-growth mechanism and the other principles provided elsewhere [52]. The specific example shown [184] illustrates the synthesis of all possible geometric isomers of a trimetallic nanocluster.

charge (inorganic; $P_2W_{15}Nb_3O_{62}^{9-}$) and steric (organic; R_4N^+) stabilization—imparts sufficient stability to the $Ir(0)_{\sim 300}$ nanoclusters such that they can be isolated as a solid, stored in a bottle, and then later redispersed *in solution* for use as an active hydrogenation catalyst [162].

Second, the $Ir(0)_{\sim 300}$ nanocluster catalysts have been shown to have the full reactivity within experimental error of the corresponding $Ir(0)/Al_2O_3$ heterogeneous catalyst *per exposed active Ir(0) atom*, demonstrating 3200 ± 1000 turnovers [mol product (mol exposed Ir(0) catalyst)$^{-1}$ h^{-1}] compared to 3950 ± 1000 turnovers for commercial 7.9% dispersed Ir/γ-Al_2O_3 or 1740 ± 250 turnovers for Exxon's 80% dispersed Ir/η-Al_2O_3 [162]. This is the first such quantitative comparison of a transition-metal nanocluster operating in solution to its heterogeneous counterpart, under the identical reaction conditions, and where the results are compared per exposed Ir atom. Moreover, initial studies showed that the $Ir(0)_{\sim 300}$ nanoclusters are capable of performing more than 18,000 turnovers over 10 days *in solution* before deactivation. This is an important result compared to all other nanocluster systems in the literature [1]. (About 10,000 turnovers are reported for Moiseev's giant palladium clusters [20], one of only two *isolable* nanocluster systems shown to do catalysis *in solution* with $\geq 10,000$ turnover lifetimes). Previously, others had stated that ''the future of large clusters in homogeneous catalysis is doubtful ... and ... the application of large clusters can be done only via the formation of heterogeneous catalysts'' [122] (i.e., by placing them on a support). *Clearly the $Ir(0)_{\sim 300}$ nanoclusters disprove this statement*, as others first noted [14,186]. The above turnovers are significant even in comparison to both traditional heterogeneous catalysts (where, for instance, under the same conditions, Exxon's 80% dispersed $Ir(0)/\eta$-Al_2O_3 dies after 20,000 turnovers). Taken together, the $\pm 15\%$ kinetic reproducibility in catalytic activity, the long lifetimes and high turnover numbers in solution, the quantitative catalyst poisoning experiments, and the potential of using spectroscopic and kinetic techniques on these 'soluble metal droplets' provide the initial evidence that these $Ir(0)_{\sim 300}$ nanoclusters act as 'soluble heterogeneous catalysts', an emerging new paradigm for catalyst materials [1].

Very recently, the $P_2W_{15}Nb_3O_{62}^{9-}$ polyoxoanion-stabilized Rh(0) nanoclusters have been shown to catalyze *190,000 total turnovers* of cyclohexene hydrogenation [187]. Hence, the nanocluster 'soluble heterogeneous catalyst' analogy [1] is now a worthy goal for additional research.

3.5.4. Is it homogeneous or heterogeneous catalysis?

A classic problem in catalysis has been how to definitively answer the several-decade-old problem of 'Is it homogeneous or heterogeneous catalysis?'. Improved methodology was reported in 1994 to answer this question, methodology which includes TEM, kinetics, quantitative poisoning experiments and the tenet that the correct mechanism will explain *all* of the data [162], Fig. 21. Notably, this methodology was developed hand-in-hand with (i.e., was the methodology behind) the discovery of polyoxoanion-stabilized nanocluster chemistry [162]. More recently these same methods, Fig. 23, have been used to show that a benzene hydrogenation catalyst, first postulated in the literature as a homogeneous '$[(C_8H_{17})_3NCH_3]^+[RhCl_4]^-$ ion-pair' catalyst, is, actually, a distribution of Rh(0) nanoclusters [188]. The important finding of $Rh(0)_n$ nanoclusters in an ostensibly '$RhCl_4^-$' catalyzed reaction demonstrates the efficacy of the new 'homogeneous-or-heterogeneous?' methodology applied to catalyst systems in the literature, that is, outside the realm within which it was developed [162]. It also shows the potential that nanoclusters hold in becoming active catalysts for arene selective hydrogenation to cyclohexene, a significant industrial reaction [189].

It is likely that the use of the methods shown in Fig. 21 [162] will lead to the discovery of nanoclusters in other reactions under reducing or other conditions in many examples of what are thought to be 'homogeneous', mono-metallic catalysts. A few cases where one can now suspect

Catalyst Isolation and
Characterization Studies,
Emphasizing Early TEM
Studies

1

Additional Mechanistic
Studies, Emphasizing
that the *Correct Mechanism
will Explain <u>All</u> the Data*

4

The
Catalyst
Material

2

Kinetic Studies Emphasizing:
 (i) Can the Isolated Catalyst
Account for the Observed Kinetics?;
(ii) Quantitative Explanation of
 any Induction Periods; and
(ii) Reproducibility (Is it $\leq \pm 10\%$?)

3

Quantitative Phenomenological
Tests, Especially Quantitative
Catalyst Poisioning and
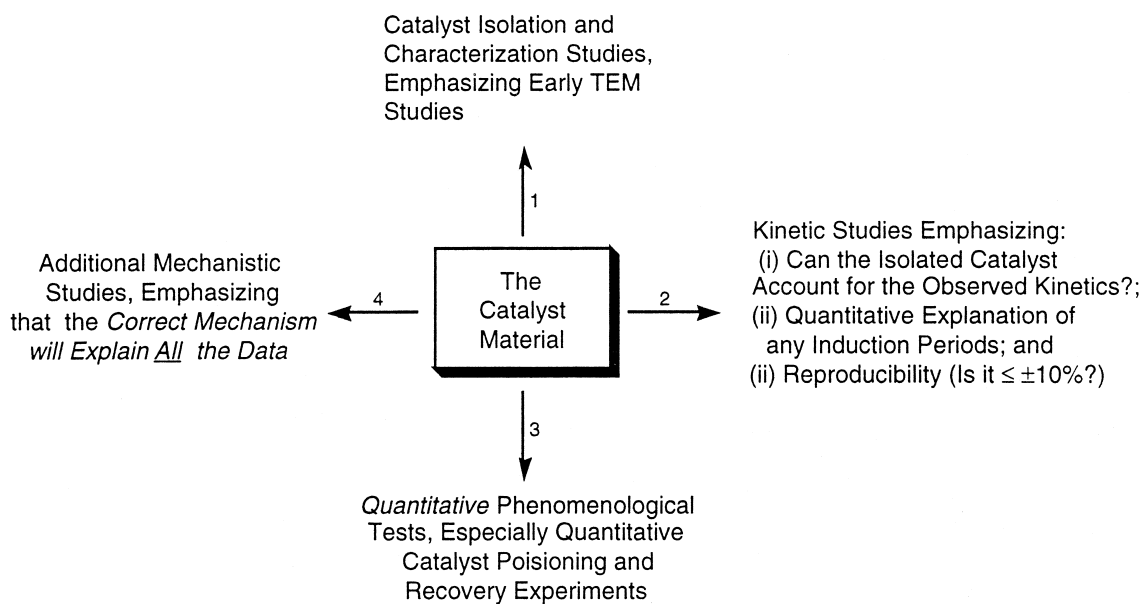Recovery Experiments

Fig. 23. Four-step method, refined during the development of polyoxoanion-nanocluster chemistry and first reported in 1994, for distinguishing between heterogeneous and homogeneous catalysis. A more detailed version of this methodology is available elsewhere [162].

nanoclusters as the true catalysts, and based on recent experience interpreting properly key observations such as induction periods or insoluble metal formation [162,188], are summarized in Refs. [190–194].

4. A summary of transition-metal nanocluster catalyst systems

Five literature systems, Table 1, from among those available for discussion, Tables 2 and 3, have been highlighted. A more complete summary of transition metal nanocluster catalysis to date is provided by Table 2, which emphasizes nanocluster systems that exhibit (homogeneous) catalysis while dissolved in solution, and by Table 3, which emphasizes systems that demonstrate (heterogeneous) catalysis once the transition-metal nanoclusters have been immobilized on a solid support. With the exception of two cases [59,195], all of the data shown in Tables 2 and 3 are taken from the five case studies described herein.

The data in these tables show the following: (i) the majority of effort has been invested in immobilized nanocluster catalysts, although reports of solution-based nanocluster catalysis (nanocluster 'soluble heterogeneous catalysts') are becoming more frequent; (ii) when nanocluster catalysts are used in solution, emphasis has been placed on merely demonstrating catalysis, rather than achieving high activity or long lifetimes; (iii) the highest demonstrated lifetime of a nanocluster catalyst in solution previously was 18,000, and now is 190,000, turnovers [187], while all others have been shown to perform only ca. 2300–10,000 when in solution (and more often ≤ 50 turnovers); (iv) typically, turnover frequencies and catalyst lifetimes are not corrected for the number of exposed metal atoms, although future studies need to strive to do this, and (v) only in a few cases are nanocluster catalysts compared directly to their respective commercial heterogeneous counterparts

Table 2
Summary of transition metal nanocluster catalysts *in solution*

Nanocluster catalyst type	Solution only or also immobilized?	Reaction/rate/turnover data	Reported turnover frequency	Reported lifetime	Refs.
$Pd_{\sim 561}(phen)_{\sim 60}(OAc)_{\sim 180}$ and $Pd_{\sim 561}(phen)_{\sim 60}(PF_6)_{\sim 60}$ 'giant palladium clusters' in $EtOH/CH_3CN$	Solution	Clusters catalyze a variety of hydrogenation and oxidative acetoxylation reactions; turnover frequencies that range between 0.3 and 15 h^{-1} are reported. This is the first report of a well-defined nanocluster as an active catalyst in solution.	0.3–15 h^{-1}	ca. 10,000	[20]
$Rh_{\sim 55}[P(t\text{-}Bu)_3]_{\sim 12}Cl_{\sim 20}$ clusters	Both In solution: ''Clusters prove to be good only in the anchored state … since [they] decompose rapidly in solution.''	Various hydrogenation and hydroformylation reactions at room temperature with yields ranging from ca. 40 to 100%. No lifetime data supplied, but some turnover frequencies (per mol-surface-atom) of supported Rh cluster catalysts are reported to be $> 10,000\ h^{-1}$.	$> 10,000\ h^{-1}$	–	[122]
$P_2W_{15}Nb_3O_{62}^{9-}$- and tetrabutylammonium-stabilized $Ir(0)_{\sim 300}$ nanoclusters in acetone	Solution	Cyclohexene hydrogenation at 22°C. Up to 18,000 total turnovers demonstrated with turnover frequencies of 3200 ± 1000. Material was compared to $Ir(0)$ heterogeneous catalysts which showed a turnover frequency of $3950 \pm 1000\ h^{-1}$.	$3200 \pm 1000^{b}\ h^{-1}$	18,000	[1] [162]
26 ± 4 Å 'Sulfoxide-stabilized' giant Pd clusters in DMSO	Solution	Oxidative cyclization of hydroxymethylamines with up to 50 turnovers demonstrated. The first turnover is reported to be the fastest.	–	up to 50[a]	[59]
$[Ti(0)\cdot 0.5THF]_x$ clusters in THF	Both	Hydrogenation of Ti and Zr sponges. No total turnover data reported. Reaction beginning with nanoclusters proceeds after induction periods, which vary with H_2 pressure. Loss of H_2 pressure is ca. 2 atm H_2 h^{-1}.[a]		–	[146]

80–100 Å Pd clusters in propylene carbonate	Solution	Heck reaction (C–C bond formation of halogenoaromatics with styrene) at 130–160°C over 5–65 h. No turnover data reported, but reaction yields are 40–97%.	–	< 10[a]	[23]
$R_4N^+Br^-$ stabilized Pd and Pd/Ni bimetallic clusters in dimethylacetamide	Solution	Suzuki and Heck C–C bond coupling reactions at 100–120°C. No turnover data reported.	–	–	[22]
$R_4N^+Cl^-$ stabilized Pd clusters in dimethylacetamide	Solution	Heck Reaction at 130–160°C; turnover frequency of up to 24,000 h^{-1} reported. Reaction is 97% complete in 5 min.	≤ 24,000 h^{-1}	ca. 2,000[a]	[195]
$R_4N^+Br^-$ stabilized Ti clusters in THF	Solution	McMurry-type coupling reactions. Yields are between 70–80%.	–	< 1[a]	[21]
15–40 Å Pt cinchonidine-stabilized clusters in HOAc/MeOH	Solution	Enantioselective hydrogenation of ethylpyruvate. Turnover frequencies are ca. 1 s^{-1}, with ca. 2300 turnovers demonstrated.	ca. 3,900 h^{-1}	≥ 2,300[a]	[16]
200 to 560 Å bimetallic Au–Pd clusters	Both	Hydrogenation of hex-2-yne. No quantitative lifetime data was reported, but 'stabilized' were more long-lived than 'unprotected' catalysts when deposited on a support.			[125]
25 Å $R_4N^+Br^-$ stabilized Ni clusters in toluene	Both	[3 + 2]cycloaddition of methylenecyclopropane to methyl acrylate at 130–140°C over 24–48 h. In solution: 29–39 turnovers demonstrated. Immobilized: 1–7 turnovers demonstrated.	–	≥ 29–39 1–7	[24]
$P_2W_{15}Nb_3O_{62}^{9-}$- and tetrabutylammonium-stabilized Rh nanoclusters in acetone	Solution	Hydrogenation of cyclohexene at room temperature. Up to 190,000 turnovers demonstrated.	–	≤ 190,000	[187]

[a]Calculated using the data provided.
[b]Corrected for the number of exposed Ir(0) atoms.

Table 3
Summary of transition metal nanocluster catalysts *immobilized on a solid support* prior to catalysis

Nanocluster catalyst type	Immobilized only or also in solution?	Reaction/rate/turnover data	Reported turnover frequency	Reported lifetime	Refs.
Various $R_4N^+ X^-$ stabilized clusters of group 6–10 metals including Pd, Co,Rh,Ru, and Pt (X = Cl, Br, I)	Immobilized	Various hydrogenation reactions; activity of immobilized nanocluster catalysts found to be better than commercial heterogeneous catalysts of the same metal.		–	[137,138]
Supported $Rh_{\sim 55}$ clusters	Immobilized	Hydroformylation of ethene and propene: 290 g propanol prepared from 1 g catalyst (1% wt. of cluster); 3000 g butanal by 1.5 g catalyst (1% weight of cluster). This corresponds, by our calculation, to ca. 430,000 turnovers, with reported frequencies of 400–600 min^{-1}. Immobilized catalyst is deactivated at 130°C.	24,000–36,000 h^{-1}	440,000[a]	[109]
Mixture of 31.5 and 36 Å, 7 and 8 shell $Pd_{\sim 561}$ clusters	Immobilized	Olefin hydrogenation; no turnover data (frequencies or lifetimes) reported.	–	–	[123]
Various $R_4N^+ X^-$ stabilized clusters of group 6–10 metals including Pd, Co, Rh, Ru, and Pt (X = Cl, Br, I)	Immobilized In solution: Ni and Pd clusters precipitate to metal within minutes (initial rates are as high as 1169 N ml H_2 g^{-1} min^{-1}, however).	Various hydrogenation reactions; some immobilized nanocluster catalysts show induction periods. Total turnovers reported for *immobilized nanocluster Pd* on carbon is 96,000 (uncorrected for the actual number of exposed Pd atoms), while commercial Pd/C showed only 38,000 turnovers (corrected for the number of exposed Pd atoms).		96,000	[139,140]

$R_4N^+X^-$ stabilized Pd clusters (X = Cl, Br, I)	Immobilized In solution: Pd clusters precipitate to metal within minutes.	1,5-Cyclooctadiene or cyclohexene hydrogenation. Pretreatment of clusters with H_2 before immobilization increases activity; pretreatment afterwards decreases activity. Total turnovers reported for immobilized colloidal Pd on carbon is 96,000. Various other immobilized cluster catalysts show maxima of between 20,000 and 50,000 turnovers.	≤ 826 N ml H_2 g^{-1} min^{-1}	20,000–50,000 96,000	[140]
$R_4N^+Br^-$ stabilized Pd clusters	Immobilized	1,5-Cyclooctene hydrogenation; activity was tested, and some colloidal catalysts were shown to be more active than their commercial heterogeneous counterparts.	–	–	[157]
$R_4N^+X^-$ stabilized Pd, Rh, and Pt clusters (X = Cl, Br)	Immobilized In solution: Pt colloids precipitates when H_2 pressure is applied.	Various hydrogenation reactions are reported but without any additional lifetime data. Oxidation of D-glucose also reported.	≤ 263 N ml H_2 g^{-1} min^{-1}	–	[57]
7 and 8 shell Pd clusters and Rh clusters, stabilized	Immobilized	Alkyne hydrogenation with turnover frequencies between 0.75–46 min^{-1} are reported, with ca. 6000 total turnovers demonstrated for the Rh example. Effect of stabilizing ligand on selectivity is examined.	45–2760 h^{-1}	6000[a]	[124]
Pt and Au or Pd bimetallic clusters	Immobilized	Hydrosilylation of 1-octene. The activity of the supported catalysts is the same over 6 cycles of reuse at 60°C.	–	–	[115]
$R_4N^+Cl^-$ stabilized Pd–Pt alloy clusters	Immobilized	Selective oxidation of glucose. No quantitative lifetime data reported, but immobilized catalysts were active over 25 reaction runs.	≤ 1607 N ml O_2 mmol $(Pd^- + Pt)^{-1}$ min^{-1}	–	[148]

[a]Calculated using the data provided.

under the identical reaction conditions, another type of comparison and control experiment worth emphasizing in the future.

5. A look towards the future

Rapid progress has been made in the nanocluster research area during only the past 5 to 10 years; however, it seems clear that much more is likely to come.

One ultimate goal of research in this area is the possibility of more active, longer-lived, possibly highly selective catalysts leading to products or knowledge that will benefit consumer technology. Other goals are also apparent, and should probably include the following.

· Large-scale (i.e., multigram, and eventually hundreds-of-grams scale) syntheses of nanocluster materials that are *both* isolable, and yet retain their full catalytic activity.

· Additional fundamental studies of nanocluster stability, leading to nanoclusters with increased temperature stability in solution, perhaps achieved by using the appropriate stabilizing polyoxo- or other poly-anions, cations (including polycations), solvents, and mixtures thereof.

· Reactivity tests, probing for unique activities and especially high selectivities not observed in traditional heterogeneous catalytic systems, especially as a function of the anionic ligand and other nanocluster-stabilizing ligands. The highly ligand-dependent selectivities Schmid has demonstrated are important in this regard [14].

· Improved characterization of nanoclusters, and more importantly, improved characterization *of their surfaces*, their surface-to-ligand interactions, and of the different types of surface atoms present (ad-atoms, edges, kinks, or planar surfaces). Such knowledge would aid in understanding the important processes such as stabilization and catalysis that occur on the metal surface of the cluster.

· The exploitation of the advantages that *soluble* nanoclusters provide, in terms of powerful solution spectroscopic and kinetic probes, to attack the surface reactivity intermediates and C, H, N, O, X and other 'overlayers' problem, an area where a heterogeneous catalysis expert notes that ''one of the puzzles of heterogeneous catalysis has been that of the absorbate overlayer'' [196].

· Additional kinetic and mechanistic studies of nanocluster formation and growth should help provide further control over particle size, shape, and composition.

· Product, then kinetic and mechanism studies, of nanocluster catalyst agglomeration or other deactivation processes, all ideally under *catalytic* reaction conditions.

· Greater studies of heterobimetallic, heterotrimetallic, and higher multimetallic nanoclusters (see the references and Scheme 2 elsewhere [184]). Especially important may be studies of enhanced selectivity, activity and lifetime/stability of polymetallic nanoclusters.

· Studies of nanoclusters in combination with other materials to make unusual types of catalysts, for example, the recent report of nanoclusters encapsulated in dendrimer templates [35].

· Studies of nanoclusters after catalysis [59], and especially of their *deactivated forms*, information which should prove crucial to designing longer-lived nanocluster catalysts, and information which may also be useful to heterogeneous metal-particle catalysts as well.

· Ultimately, perhaps, the use of nanoclusters to develop *single-active site* heterogeneous catalysts, ones that may have *selectivities approaching 100%*, two of the goals in the Vision 2020 report on catalysis [197].

Overall, it seems clear that fundamental studies of nanocluster syntheses, characterization, and stabilization, and the exploitation of such materials in practical applications such as catalysis, hold

much promise for further advances. Hence, it seems likely that this area will continue to produce exciting results for years to come.

Acknowledgements

References

[1] J.D. Aiken III, Y. Lin, R.G. Finke, J. Mol. Catal. A: Chem. 114 (1996) 29–51.
[2] G. Schmid (Ed.), Clusters and Colloids: From Theory to Applications, VCH Publishers, New York, 1994.
[3] L.J. de Jongh (Ed.), Physics and Chemistry of Metal Cluster Compounds, Kluwer Publishers, Dordrecht, 1994.
[4] R. Pool, Clusters: strange morsels of matter, Science 248 (1990) 1186–1188.
[5] U. Simon, G. Schön, G. Schmid, Angew. Chem., Int. Ed. Engl. 32 (1993) 250.
[6] J. Glanz, Science 269 (1995) 1363.
[7] G. Schön, U. Simon, Colloid Polym. Sci. 273 (1995) 202.
[8] M. Antonietti, C. Göltner, Angew. Chem., Int. Ed. Engl. 36 (1997) 910–928.
[9] R. Elghanian, J.J. Storhoff, R.C. Mucic, R.L. Letsinger, C.A. Mirkin, Science 277 (1997) 1078.
[10] V.L. Colvin, M.C. Schlamp, A.P. Alivisatos, Nature 370 (1994) 354–357.
[11] S.V. Sonti, A. Bose, J. Colloid Interface Sci. 170 (1995) 575.
[12] M.T. Reetz, M. Winter, G. Dumpich, J. Lohau, S. Friedrichowski, J. Am. Chem. Soc. 119 (1997) 4539–4540.
[13] T. Vossmeyer, E. DeIonno, J.R. Heath, Angew. Chem., Int. Ed. Engl. 36 (1997) 1080.
[14] G. Schmid, V. Maihack, F. Lantermann, S. Peschel, J. Chem. Soc., Dalton Trans. (1996) 589.
[15] Y. Lin, R.G. Finke, J. Am. Chem. Soc. 116 (1994) 8335–8353.
[16] Bönnemann, G.A. Braun, Angew. Chem., Int. Ed. Engl. 35 (1996) 1992.
[17] L.N. Lewis, N. Lewis, J. Am. Chem. Soc. 108 (1986) 7228–7231. (See, however, J. Stein, L.N. Lewis, Y. Gao, R.A. Scott, J. Am. Chem. Soc. 121 (1999) 3693–3703).
[18] J.P. Wilcoxon, T. Martino, E. Klavetter, A.P. Sylwester, Nanophase Mater. (1994) 771–780.
[19] T.J. Schmidt, M. Noeske, H.A. Gasteiger, R.J. Behm, P. Britz, W. Brijoux, H. Bönnemann, Langmuir 13 (1997) 2591.
[20] M.N. Vargaftik, V.P. Zargorodnikov, I.P. Stolarov, I.I. Moiseev, D.I. Kochubey, V.A. Likholobov, A.L. Chuvilin, K.I. Zamaraev, J. Mol. Catal. 53 (1989) 315–348.
[21] M.T. Reetz, S.A. Quaiser, C. Merk, Chem. Ber. 129 (1996) 741–743.
[22] M.T. Reetz, R. Breinbauer, K. Wanninger, Tetrahedon Lett. 37 (1996) 4499–4502.
[23] M.T. Reetz, G. Lohmer, J. Chem. Soc., Chem. Commun. (1996) 1921–1922.
[24] M.T. Reetz, R. Breinbauer, P. Wedemann, P. Binger, Tetrahedron 54 (1998) 1233–1240.
[25] J.P. Wilcoxon, A. Martino, R.L. Baughmann, E. Klavetter, A.P. Sylwester, Mater. Res. Soc. Symp. Proc. 286 (1993) 131.
[26] J.P. Wilcoxon, R.L. Williamson, R. Baughman, J. Chem. Phys. 98 (1993) 9933–9949.
[27] J.P. Wilcoxon, T. Martino, E. Klavetter, A.P. Sylwester, Nanophase Mater. (1994) 771–780.
[28] E.L. Venturini, J.P. Wilcoxon, P.P. Newcomer, Mater. Res. Soc. Symp. Proc. 351 (1994) 311.
[29] F. Parsapour, D.F. Kelley, S. Craft, J.P. Wilcoxon, J. Phys. Chem. 104 (1996) 4978.
[30] J.P. Wilcoxon, P.P. Newcomer, G.A. Samara, J. Appl. Phys. 81 (1997) 7934.
[31] M.L. Steigerwald, L.E. Brus, Acc. Chem. Res. 23 (1990) 183–188.
[32] N.L. Pocard, D.C. Alsmeyer, R.L. McCreery, T.X. Neenan, M.R. Callstrom, J. Am. Chem. Soc. 114 (1992) 769–771.
[33] Y. Ng Cheomg Chan, R.R. Schrock, R.E. Cohen, Chem. Mater. 4 (1992) 205–211.
[34] Y. Ng Cheomg Chan, R.R. Schrock, R.E. Cohen, J. Am. Chem. Soc. 114 (1992) 7290–7296.
[35] M. Zhao, L. Sun, R.M. Crooks, J. Am. Chem. Soc. 120 (1998) 4877–4878.
[36] M. Meyer, C. Wallberg, K. Kurihara, J.H. Fendler, J. Chem. Soc., Chem. Commun. 90 (1984) 90.
[37] C. Petit, M.P. Pileni, J. Phys. Chem. 92 (1988) 2282.
[38] C. Petit, P. Lixon, M.P. Pileni, J. Phys. Chem. 94 (1990) 1598.
[39] M.P. Pileni, Adv. Colloid Interface Sci. 46 (1993) 139.
[40] C. Sangregotio, M. Galeotti, U. Bardi, P. Baglioni, Langmuir 12 (1996) 6326.
[41] M.L. Steigerwald, L.E. Brus, Acc. Chem. Res. 23 (1990) 183–188.
[42] I. Lisiecki, M.P. Pileni, J. Am. Chem. Soc. 115 (1993) 3887.
[43] I. Lisiecki, M.P. Pileni, J. Phys. Chem. 99 (1995) 5077.

[44] I. Lisiecki, F. Billoudet, M.P. Pileni, J. Phys. Chem. 100 (1996) 4160.
[45] A.R. Kortan, R. Hull, R.L. Opila, M.G. Bawendi, M.L. Steigerwald, P.J. Carroll, L.E. Brus, J. Am. Chem. Soc. 112 (1990) 1327–1332.
[46] A. Martino, S.A. Yamanaka, J.S. Kawola, D.A. Loy, Chem. Mater. 9 (1997) 423–429.
[47] K. Kon-No, in: K. Esumi, M. Ueno (Eds.), Structure–Performance Relationships in Surfactants: Surfactant Science Series, Vol. 70, Chap. 13, Marcel Dekker, 1997.
[48] G. Schmid (Ed.), Clusters and Colloids: From Theory to Applications, Chap. 6, VCH Publishers, New York, 1994.
[49] T.S. Ahmadi, Z.L. Wang, A. Henglein, M.A. El-Sayed, Chem. Mater. 8 (1996) 161.
[50] J.M. Petroski, Z.L. Wang, T.C. Green, M.A. El-Sayed, J. Phys. Chem. B 102 (1998) 3316.
[51] T.S. Ahmadi, Z.L. Wang, T.C. Green, A. Henglein, M.A. El-Sayed, Science 272 (1996) 1924.
[52] M.A. Watzky, R.G. Finke, J. Am. Chem. Soc. 119 (1997) 10382–10400.
[53] T. Teranishi, M. Miyake, Size control of palladium nanoparticles and their crystal structures, Chem. Mater. 10 (1998) 594–600.
[54] R.J. Hunter, Foundations of Colloid Science, Vol. 1, Oxford Univ. Press, New York, 1987.
[55] A.J. Bard, L.R. Faulkner, Electrochemical Methods, Wiley, New York, 1980.
[56] D.H. Napper, Polymeric Stabilization of Colloidal Dispersions, Academic Press, London, 1983.
[57] H. Bönnemann, G. Braun, W. Brijoux, R. Brinkmann, A. Schulze Tilling, K. Seevogel, K. Siepen, J. Organomet. Chem. 520 (1996) 143–162.
[58] C.S. Hirtzel, R. Rajagopalan, Colloidal Phemonena: Advanced Topics, 1985, pp. 27–39, pp. 73–87.
[59] R.A.T.M. van Benthem, H. Heimstra, P.W.N.M. van Leeuwen, J.W. Geus, W.N. Speckamp, Angew. Chem., Int. Ed. Engl. 34 (1995) 547.
[60] G. Schmid, Endeavour, New Series 14 (1990) 172–178.
[61] Y. Iwasawa (Ed.), Tailored Metal Catalysts, Kluwer, Dordrecht, 1986.
[62] G. Schmid (Ed.), Clusters and Colloids: From Theory to Applications, VCH Publishers, New York, 1994, p. 183.
[63] H. Weller, Angew. Chem., Int. Ed. Engl. 35 (1996) 1079–1081.
[64] D.B. Williams, C.B. Carter, Transmission Electron Microscopy, A Textbook for Materials Science, Plenum, New York, 1996.
[65] G. Schmid, Struct. Bonding 62 (1985) 51–85.
[66] G. Schmid, Polyhedron 7 (1988) 2321–2329.
[67] G. Schmid, Chem. Rev. 92 (1992) 1709–1727.
[68] M. Che, C.O. Bennet, Adv. Catal. 36 (1989) 55.
[69] V.V. Volkov, G. Van Tendeloo, G.A. Tsirkov, N.V. Cherkashina, M.N. Vargaftik, I.I. Moiseev, V.M. Novotortsev, A.V. Kvit, A.L. Chuvilin, J. Cryst. Growth 163 (1996) 377.
[70] J.A. Creighton, D.G. Eadon, J. Chem. Soc., Faraday Trans. 87 (1991) 3881.
[71] N. Chestnoy, T.D. Harris, R. Hull, L.E. Brus, J. Phys. Chem. 90 (1986) 3393–3399.
[72] M.T. Reetz, in: A. Fürstner (Ed.), Active Metals, VCH, Weinheim, 1996, pp. 279–297.
[73] G. Schmid (Ed.), Clusters and Colloids: From Theory to Applications, VCH Publishers, New York, 1994, p. 506.
[74] G. Schmid (Ed.), Clusters and Colloids: From Theory to Applications, VCH Publishers, New York, 1994, p. 507.
[75] J.S. Bradley, J.M. Millar, E.W. Hill, J. Am. Chem. Soc. 113 (1991) 4016–4017.
[76] J.S. Bradley, E.W. Hill, S. Behal, C. Klein, B. Chaudret, A. Duteil, Chem. Mater. 4 (1992) 1234.
[77] J.S. Bradley, E.W. Hill, C. Klein, B. Chaudret, A. Duteil, Chem. Mater. 5 (1993) 254–256.
[78] A. Duteil, R. Queau, B. Chaudret, R. Mazel, C. Roucau, J.S. Bradley, Chem. Mater. 5 (1993) 341–347.
[79] J.S. Bradley, G.H. Via, L. Bonneviot, E.W. Hill, Chem. Mater. 8 (1996) 1895.
[80] A. Rodriguez, C. Amiens, B. Chaudret, M.-J. Casanove, P. Lecante, J.S. Bradley, Chem. Mater. 8 (1996) 1978.
[81] D. de Caro, J.S. Bradley, Langmuir 13 (1997) 3067.
[82] D. de Caro, J.S. Bradley, Chem. Mater. 14 (1998) 245–247.
[83] R.M. Mucalo, R.P. Cooney, J. Chem. Soc., Faraday Trans. 87 (1991) 1221–1227.
[84] G. Schmid (Ed.), Clusters and Colloids: From Theory to Applications, VCH Publishers, New York, 1994, p. 467.
[85] M. Kerker, O. Siman, L.A. Bumm, W.-S. Wang, Appl. Opt. 19 (1980) 3253–3255.
[86] G. Schmid (Ed.), Clusters and Colloids: From Theory to Applications, VCH Publishers, New York, 1994, p. 510.
[87] A. Badia, L. Cuccia, L. Demers, F. Morin, B. Lennox, J. Am. Chem. Soc. 119 (1997) 2682–2692.
[88] A. Badia, L. Demers, L. Dickenson, F.G. Morin, R.B. Lennox, L. Reven, J. Am. Chem. Soc. 119 (1997) 11104–11105.
[89] G. Schmid, Struct. Bonding 62 (1985) 51–85.
[90] G. Schmid (Ed.), Clusters and Colloids: From Theory to Applications, VCH Publishers, New York, 1994, p. 23.
[91] G. Schmid (Ed.), Clusters and Colloids: From Theory to Applications, VCH Publishers, New York, 1994, p. 516.
[92] R. Wiesendanger, Scanning Probe Microscopy and Spectroscopy, Methods and Applications, Cambridge Univ. Press, Cambridge, 1994.
[93] H. van Kempen, J.G.A. Dubois, J.W. Gerritsen, G. Schmid, Physica B 204 (1995) 51.
[94] R. Houbertz, T. Feigenspan, F. Mielke, U. Memmert, U. Hartmann, U. Simon, G. Schön, G. Schmid, Europhys. Lett. 28 (1994) 641.
[95] M.S. Kaba, I.K. Song, D.C. Duncan, C.L. Hill, M.A. Barteau, Inorg. Chem. 37 (1998) 398.
[96] H.A. Wierenga, L. Soethout, J.W. Gerritsen, B.E.C. van de Leemput, H. van Kempen, G. Schmid, Adv. Mater. 2 (1990) 482.
[97] C. Becker, T. Fries, K. Wandelt, J. Vac. Sci. Technol. B 9 (1991) 810.

[98] Y. Wang, Q. Xu, Y. Xie, L. Gui, Y. Tang, J. Colloid Interface Sci. 151 (1992) 392.
[99] M.T. Reetz, W. Helbig, S.A. Quaiser, U. Stimming, N. Breuer, R. Vogal, Science 267 (1995) 367–369.
[100] P. Mulvaney, M. Giersig, J. Chem. Soc., Faraday Trans. 92 (1996) 3137.
[101] G. Schmid, S. Peschel, New J. Chem. 22 (1998) 669–675.
[102] G. Schmid, R. Pfeil, R. Boese, F. Bandermann, S. Meyer, G.H.M. Calis, J.A.W. van der Velden, Chem. Ber. 114 (1981) 3634–3642.
[103] G. Schmid, Polyhedron 7 (1988) 2321–2329.
[104] L.J. de Jongh, J.A.O. de Aguiar, H.B. Brom, G. Longoni, J.M. vanRuitenbeek, G. Schmid, H.H.A. Smit, M.P.J. van Staveren, R.C. Thiel, Z. Phys. D: At., Mol. Clusters 12 (1989) 445–450.
[105] K. Fauth, U. Kreibig, G. Schmid, Z. Phys. D: At., Mol. Clusters 12 (1989) 515–520.
[106] G. Schmid, B. Morum, J. Malm, Angew. Chem., Int. Ed. Engl. 28 (1989) 778–780.
[107] G. Schmid, N. Klein, L. Korste, Polyhedron 7 (1988) 605–608.
[108] T. Tominaga, S. Tenma, H. Watanabe, U. Giebel, G. Schmid, Chem. Lett. (1996) 1033.
[109] G. Schmid, Chem. Rev. 92 (1992) 1709–1727.
[110] H.A. Wierenga, L. Soethout, J.W. Gerritsen, B.E.C. van de Leemput, H. van Kempen, G. Schmid, Adv. Mater. 2 (1990) 482.
[111] R. Houbertz, T. Feigenspan, F. Mielke, U. Memmert, U. Hartmann, U. Simon, G. Schon, G. Schmid, Europhys. Lett. 28 (1994) 641.
[112] L.E.C. van de Leemput, J.W. Gerritsen, P.H.H. Rongen, R.T.M. Smokers, H.A. Wierenga, H. van Kempen, J. Vac. Sci. Technol. B 9 (1991) 814–819.
[113] H. van Kempen, J.G.A. Dubois, J.W. Gerritsen, G. Schmid, Physica B 204 (1995) 51.
[114] M.P.J. van Staveren, H.B. Brom, L.J. de Jongh, G. Schmid, Z. Phys. D: At., Mol. Clusters 12 (1989) 451–452.
[115] G. Schmid, H. West, H. Mehles, A. Lehnert, Inorg. Chem. 36 (1997) 891–895.
[116] G. Schmid, N. Klein, B. Morun, A. Lehnert, Pure Appl. Chem. 62 (1990) 1175–1177.
[117] G. Schmid, A. Lehnert, Angew. Chem., Int. Ed. Engl. 28 (1989) 780–781.
[118] R.E. Benfield, J.A. Creighton, D.G. Eadon, G. Schmid, Z. Phys. D: At., Mol. Clusters 12 (1989) 533–536.
[119] G. Schmid, Mater. Chem. Phys. 29 (1991) 133–142.
[120] R.S. Drago, Physical Methods for Chemists, 2nd edn., Harcourt Brace Jovanovich, New York, 1992.
[121] B.A. Smith, J.Z. Zhang, U. Giebel, G. Schmid, Chem. Phys. Lett. 270 (1997) 139–144.
[122] G. Schmid, in: R. Ugo (Ed.), Aspects of Homogeneous Catalysis, Vol. 7, Kluwer Academic Publishers, 1990, pp. 1–33.
[123] G. Schmid, M. Harms, J.-O. Malm, J.-O. Bovin, J. van Ruitenbeck, H.W. Zandbergen, W.T. Fu, J. Am. Chem. Soc. 115 (1993) 2046.
[124] G. Schmid, V. Maihack, F. Lantermann, S. Peschel, J. Chem. Soc., Dalton Trans. (1996) 589–595.
[125] G. Schmid, H. West, J.-O. Malm, J.-O. Bovin, C. Grenthe, Chem.: A Eur. J. 2 (1996) 1099.
[126] G. Schmid, S. Peschel, T. Sawitowski, Z. Anorg. Allg. Chem. 623 (1997) 719–723.
[127] A. Bezryadin, C. Dekker, G. Schmid, Appl. Phys. Lett. 71 (1997) 1273.
[128] G. Schmid, J. Chem. Soc., Dalton Trans. (1998) 1077–1082.
[129] U. Simon, R. Flesch, H. Wiggers, G. Schön, G. Schmid, J. Mater. Chem. 8 (1998) 517–518.
[130] S. Peschel, G. Schmid, Angew. Chem., Int. Ed. Engl. 34 (1995) 1442.
[131] G. Hornyak, M. Kröll, R. Pugin, T. Sawitowski, G. Schmid, J.-O. Bovin, G. Karsson, H. Hofmeister, S. Hopfe, Chem. Eur. J. 3 (1997) 1951–1956.
[132] M.N. Vargaftik, V.P. Zargorodnikov, I.P. Stolarov, I.I. Moiseev, V.A. Likholobov, D.I. Kochubey, A.L. Chuvilin, V.I. Zaikosvsky, K.I. Zamaraev, G.I. Timofeeva, J. Chem. Soc., Chem. Commun. (1985) 937–939.
[133] V.V. Volkov, G. Van Tendeloo, G.A. Tsirkov, N.V. Cherkashina, M.N. Vargaftik, I.I. Moiseev, V.M. Novotortsev, A.V. Kvit, A.L. Chuvilin, J. Cryst. Growth 163 (1996) 377.
[134] I.I. Moiseev, M.N. Vargaftik, V.V. Volkov, G.A. Tsirkov, N.V. Cherkashina, V.M. Novotortsev, O.G. Ellert, I.A. Petrunenka, A.L. Chuvilin, A.V. Kvit, Mend. Commun. (1995) 87.
[135] V. Oleshko, V. Volkov, W. Jacob, M. Vargaftik, I. Moiseev, G. Van Tendeloo, Z. Phys. D 34 (1995) 283.
[136] I.I. Moiseev, M.N. Vargaftik, T.V. Chernysheva, T.A. Stromnova, A.E. Gekhman, G.A. Tsirkov, A.M. Makhlina, J. Mol. Catal. A: Chem. 108 (1996) 77.
[137] H. Bönnemann, W. Brijoux, R. Brinkmann, E. Dinjus, T. Jouben, B. Korall, Angew. Chem., Int. Ed. Engl. 30 (1991) 1312–1314.
[138] H. Bönnemann, W. Brijoux, R. Brinkmann, E. Dinjus, R. Fretzen, T. Jouben, B. Korall, J. Mol. Catal. 74 (1992) 323.
[139] H. Bönnemann, W. Brijoux, R. Brinkmann, R. Fretzen, T. Joussen, R. Koppler, B. Korall, P. Neiteler, J. Richter, J. Mol. Catal. 86 (1994) 129.
[140] H. Bönnemann, R. Brinkmann, P. Neiteler, Appl. Organomet. Chem. 8 (1994) 361.
[141] H. Bönnemann, W. Brijoux, in: A. Fürstner (Ed.), Active Metals: Preparation, Characterization, Applications, VCH, New York, 1996, pp. 339–379.
[142] H. Bönnemann, R. Brinkmann, R. Koppler, P. Neiteler, J. Richter, Adv. Mater. 4 (1992) 804–806.
[143] J. Rothe, J. Pollmann, R. Franke, J. Hormes, H. Bönnemann, W. Brijoux, K. Siepen, J. Richter, Fresenius' J. Anal. Chem. 355 (1996) 372.
[144] J. Rothe, J. Hormes, H. Bönnemann, W. Brijoux, K. Siepen, J. Am. Chem. Soc. 120 (1998) 6019–6023.
[145] R. Franke, J. Rothe, J. Pollmann, J. Hormes, H. Bönnemann, W. Brijoux, T. Hindenburg, J. Am. Chem. Soc. 118 (1996) 12090–12097.

[146] H. Bönnemann, W. Brijoux, Nanostruct. Mater. 5 (1995) 135–140.
[147] B.C. Gates, Chem. Rev. 95 (1995) 511–522.
[148] H. Bönnemann, W. Brijoux, R. Brinkmann, A. Schilze Tilling, T. Schilling, B. Tesche, K. Seevogel, R. Franke, J. Hormes, G. Köhl, J. Pollmann, J. Rothe, W. Vogel, Inorg. Chim. Acta 270 (1998) 95–110.
[149] M.T. Reetz, W. Helbig, S.A. Quaiser, in: A. Fürstner (Ed.), Active Metals: Preparation, Characterization, Applications, VCH, New York, 1996.
[150] M.T. Reetz, W. Helbig, J. Am. Chem. Soc. 116 (1994) 7401–7402.
[151] M.T. Reetz, W. Helbig, J. Am. Chem. Soc. 116 (1994) 7401–7402.
[152] M.T. Reetz, S.A. Quaiser, Angew. Chem., Int. Ed. Engl. 34 (1995) 2240.
[153] M.T. Reetz, W. Helbig, S.A. Quaiser, Chem. Mater. 7 (1995) 2227.
[154] U. Kolb, S.A. Quaiser, M. Winter, M.T. Reetz, Chem. Mater. 8 (1996) 1889.
[155] M. Mostafavi, J.L. Marignier, J. Amblard, J. Belloni, Z. Phys. D: At., Mol. Clusters 12 (1989) 31–35.
[156] M. Mostafavi, J.L. Marignier, J. Amblard, J. Belloni, J. Radiat. Phys. Chem. 34 (1989) 605–617.
[157] M.T. Reetz, S.A. Quaiser, R. Breinbauer, B. Tesche, Angew. Chem., Int. Ed. Engl. 34 (1995) 2728–2730.
[158] J.A. Becker, R. Schafer, J.R. Festag, J.H. Wendorff, F. Hensel, J. Pebler, S.A. Quaiser, W. Helbig, M.T. Reetz, Surf. Rev. Lett. 3 (1996) 1121–1126.
[159] M.T. Reetz, S.A. Quaiser, M. Winter, J.A. Becker, R. Schafer, U. Stimming, A. Marmann, R. Vogel, T. Konno, Angew. Chem., Int. Ed. Engl. 35 (1996) 2092.
[160] J. Lohau, S. Friedrichowski, G. Dumpich, E.F. Wassermann, M. Winter, M.T. Reetz, J. Vac. Sci. Technol. B 16 (1998) 77–79.
[161] M.T. Reetz, M. Winter, B. Tesche, J. Chem. Soc., Chem. Commun. (1997) 147–148.
[162] Y. Lin, R.G. Finke, Inorg. Chem. 33 (1994) 4891–4910.
[163] J.P. Fackler, C.J. McNeil, R.E.P. Winpenny, L.H. Pignolet, J. Am. Chem. Soc. 111 (1989) 6434–6435.
[164] H. Feld, A. Leute, D. Rading, A. Benninghoven, J. Am. Chem. Soc. 112 (1990) 8166–8167.
[165] D. van der Putten, R. Zanoni, C. Coluzza, G. Schmid, J. Chem. Soc., Dalton Trans. (1996) 1721.
[166] C.J. McNeal, R.E.P. Winpenny, J.M. Hughes, R.D. Macfarlane, L.H. Pignolet, L.T.J. Nelson, T.G. Gardner, L.H. Irgens, G. Vigh, J.P. Fackler, Inorg. Chem. 32 (1993) 5582.
[167] M.A. Watzky, Chem. Mater. 9 (1997) 3083–3095.
[168] G. Schmid, A. Lehnert, J.-O. Malm, J.-O. Bovin, Angew. Chem., Int. Ed. Engl. 30 (1991) 874.
[169] J. Chem. Soc., Faraday Discuss. 92 (1991) 159–172.
[170] K. Nomiya, M. Pohl, N. Mizuno, D.K. Lyon, R.G. Finke, Inorg. Synth. 31 (1997) 186–201.
[171] M. Pohl, D.K. Lyon, N. Mizuno, K. Nomiya, R.G. Finke, Inorg. Chem. 34 (1995) 1413.
[172] M. Pohl, R.G. Finke, Organometallics 12 (1993) 1453–1457.
[173] R.G. Finke, D.K. Lyon, K. Nomiya, S. Sur, N. Mizuno, Inorg. Chem. 29 (1990) 1784–1787.
[174] J.D. Aiken III, R.G. Finke, Unpublished results and experiments in progress.
[175] D.J. Edlund, PhD Dissertation, University of Oregon, 1987.
[176] M.A. Watzky, J.A. Widegren, J.D. Aiken III, R.G. Finke, manuscript in preparation.
[177] R.M. Noyes, R.J. Field, Acc. Chem. Res. 10 (1977) 214.
[178] R.M. Noyes, R.J. Field, Acc. Chem. Res. 10 (1977) 273.
[179] R.J. Field, R.M. Noyes, Nature 273 (1972) 390.
[180] M. Mostafavi, J.L. Marignier, J. Amblard, J. Belloni, J. Radiat. Phys. Chem. 34 (1989) 605–617.
[181] M. Mostafavi, J.L. Marignier, J. Amblard, J. Belloni, Z. Phys. D: At., Mol. Clusters 12 (1989) 31–35.
[182] A. Henglein, R. Tausch-Tremd, J. Colloid Interface Sci. 80 (1981) 84–93.
[183] B.G. Erskov, N.I. Kartashev, Russ. Chem. Bull. 44 (1995) 29–31.
[184] M.A. Watzky, R.G. Finke, Chem. Mater. 9 (1997) 3083–3095.
[185] X. Peng, J. Wickham, A.P. Alivisatos, J. Am. Chem. Soc. 120 (1998) 5343–5344.
[186] G. Schmid, in: B. Cornils, W.A. Herrmann (Eds.), Applied Homogeneous Catalysis with Organometallic Compounds, VCH, New York, 1996, p. 641.
[187] J.D. Aiken III, R.G. Finke, submitted for publication.
[188] K.S. Weddle, J.D. Aiken III, R.G. Finke, J. Am. Chem. Soc. 120 (1998) 5653–5666.
[189] K.S. Weddle, Masters Thesis, Colorado State University, 1997.
[190] R.A. Jones, M.H. Seeberger, J. Chem. Soc., Chem. Commun. (1985) 373.
[191] D.E. Bergbreiter, R. Chandran, J. Am. Chem. Soc. 109 (1987) 174.
[192] E. Fache, F. Senocq, C. Santini, J.-M. Basset, J. Chem. Soc., Chem. Commun. (1990) 1776.
[193] M.A. Bennett, T.-I. Huang, A.K. Smith, T.W. Turney, J. Chem. Soc., Chem. Commun. (1978) 582.
[194] J.W. Johnson, E.L. Muetterties, J. Am. Chem. Soc. 99 (1977) 7395.
[195] M. Beller, H. Fischer, K. Kuhlein, C.-P. Reisinger, W.A. Herrmann, J. Organomet. Chem. 520 (1996) 257–259.
[196] P.W. Jacobs, G.A. Somorjai, J. Mol. Catal. A: Chem. 131 (1998) 5–18.
[197] Vision 2020 Catalysis Report; http://www.chem.purdue.edu.